Redox Biology 57 (2022) 102484

Contents lists available at ScienceDirect

Redox Biology

journal homepage: www.elsevier.com/locate/redox

Sulfanegen stimulates 3-mercaptopyruvate sulfurtransferase activity and ameliorates Alzheimer's disease pathology and oxidative stress *in vivo*

Swetha Pavani Rao [a], Wei Xie [a], Ye In Christopher Kwon [b], Nicholas Juckel [b], Jiashu Xie [a], Venkateshwara Rao Dronamraju [a], Robert Vince [a], Michael K. Lee [b,c], Swati S. More [a,*]

[a] Center for Drug Design, College of Pharmacy, University of Minnesota, Minneapolis, MN, 55455, USA
[b] Department of Neuroscience, University of Minnesota, Minneapolis, MN, 55455, USA
[c] Institute for Translational Neuroscience, University of Minnesota, Minneapolis, MN, 55455, USA

ARTICLE INFO

Keywords:
Alzheimer's disease
Neuroinflammation
Neurodegeneration
3MST
Hydrogen sulfide
Sulfanegen

ABSTRACT

Increased oxidative stress and inflammation are implicated in the pathogenesis of Alzheimer's disease. Treatment with hydrogen sulfide (H_2S) and H_2S donors such as sodium hydrosulfide (NaSH) can reduce oxidative stress in preclinical studies, however clinical benefits of such treatments are rather ambiguous. This is partly due to poor stability and bioavailability of the H_2S donors, requiring impractically large doses that are associated with dose-limiting toxicity. Herein, we identified a bioavailable 3-mercaptopyruvate prodrug, sulfanegen, which is able to pose as a sacrificial redox substrate for 3-mercaptopyruvate sulfurtransferase (3MST), one of the H_2S biosynthetic enzymes in the brain. Sulfanegen is able to mitigate toxicity emanating from oxidative insults and the $A\beta_{1\text{-}42}$ peptide by releasing H_2S through the 3MST pathway. When administered to symptomatic transgenic mouse model of AD (APP/PS1; 7 and 12 months) and mice that were intracerebroventricularly administered with the $A\beta_{1\text{-}42}$ peptide, sulfanegen was able to reverse oxidative and neuroinflammatory consequences of AD pathology by restoring 3MST function. Quantitative neuropathological analyses confirmed significant disease modifying effect of the compound on amyloid plaque burden and brain inflammatory markers. More importantly, sulfanegen treatment attenuated progressive neurodegeneration in these mice, as evident from the restoration of TH+ neurons in the locus coeruleus. This study demonstrates a previously unknown concept that supplementation of 3MST function in the brain may be a viable approach for the management of AD. Finally, brought into the spotlight is the potential of sulfanegen as a promising AD therapeutic for future drug development efforts.

1. Introduction

Alzheimer's disease (AD) is the most common neurodegenerative disease and is identified by the deterioration of memory and motor functions. The neuronal damage in AD is the result of extracellular deposition of amyloid-β plaque and intraneuronal aggregation of microtubule-associated protein tau, leading to selective loss of neurons in the forebrain and other regions of brain [1,2]. AD pathogenesis is associated with increased oxidative stress and neuroinflammation, which ultimately progresses to neurodegeneration [3]. Postmortem brains of AD patients show increased levels of lipid peroxidation [4], activated microglia/astrocytes and overexpression of proinflammatory cytokines (TNF-α, IL-6) associated with senile plaques deposits [5,6]. Accumulating evidence suggest involvement of neuroinflammation during onset and exacerbation of AD pathology [7]. Imbalance in the level of hydrogen sulfide (H_2S), an endogenous anti-inflammatory neurotransmitter, is reported in the AD patient brain [8–10]. In AD patients, plasma H_2S levels inversely correlate with disease severity and cognitive function [11,12].

Supplementation of the H_2S levels by systemic sulfurous water, sublimed sulfur, or inorganic sulfite salts have provided promising results in AD animal models, but clinical efficacy studies have thus far been inconclusive [13,14]. Instability of the H_2S donors due to the ease of their oxidation and unpleasant odors of their formulations are factors that are partly responsible. These shortcomings highlight the dire need of novel approaches for restoring H_2S homeostasis and more specific drug targets.

Several physiological functions in the brain are influenced by H_2S signaling, however the underlying molecular mechanisms that H_2S recruits are incompletely understood [15]. Cellular levels of H_2S are

* Corresponding author.
E-mail address: morex002@umn.edu (S.S. More).

https://doi.org/10.1016/j.redox.2022.102484
Received 5 July 2022; Received in revised form 31 August 2022; Accepted 19 September 2022
Available online 26 September 2022

tightly controlled because excessive concentrations of this neurotransmitter can be neurotoxic and are implicated in suspended animated state due to inhibition of complex IV of the electron transport chain [16]. Physiological effects are explained by oxidative posttranslational modification of protein thiols i.e. protein persulfidation (P-SSH), caused by H_2S [17]. This mechanism contributes toward its anti-oxidant, anti-apoptotic and anti-inflammatory properties [18–21]. H_2S also modulates tissue levels of antioxidant glutathione (GSH) [18]. Neuroprotective effects of H_2S in AD are influenced by multiple pathways [22,23]. H_2S was found to inhibit expression and function of enzyme β-secretase and amyloidogenic processing of amyloid precursor protein (APP), thus reducing β-amyloid plaque burden [24]. Persulfidation of glycogen synthase kinase 3β (GSK-3β) by H_2S resulted in prevention of tau aggregation into neurofibrillary tangles in the 3xTg-AD mice [25]. Its effects on the levels of apoptotic proteins (Bcl2, Bax), anti-inflammatory cytokines (via p38-MAPK and p65-NFκB) and anti-oxidant response genes (Nrf2, heme oxygenase-1) were also noted in the APP/PS1 mouse model of AD [26,27]. While the pleiotropic activity of the gaseous transmitter H_2S has been mimicked by chemical donors providing neuroprotection, there have been limited attempts to engage the enzymatic pathways responsible for H_2S release [28,29]. Endogenous production of H_2S is driven by three biosynthetic enzymes; cystathionine γ-lyase (CSE), cystathionine β-synthase (CBS) and 3-mercaptopyruvate sulfurtransferase (3MST) [30–32]. Both CSE and CBS utilize cysteine as a precursor, while 3MST prefers 3-mercaptopyruvate as a substrate, a catabolite of cysteine produced by enzyme cysteine aminotransferase (CAT) [18,30,33]. All three enzymes are expressed widely in the brain: CBS being present in the astrocytes [34,35], CSE in the neurons [36], while 3MST is resident in both neurons and astrocytes [30,37]. While CBS and CSE are predominantly located in cytoplasm [38,39], 3MST is localized in cytoplasm and mitochondria [40–42]. This has led to proposition that being a member of the rhodanese family, 3MST could contribute toward H_2S signaling in the brain and the liberated H_2S is more readily available as bound sulfane sulfur stores compared to that by CBS [43]. It is important to note that 3MST acts in conjunction with CAT to produce H_2S and the affinity of CAT for cysteine (measured by Km) is much lower than that of CSE and CBS [17]. Thus, effective activation of 3MST could be possible either by external supplementation of 3-mercaptopyruvate or in the event of compromised CSE/CBS expression or function due to disease pathology. Downregulation of CSE has been reported in AD animal models and the human brain at advanced stages of the disease [25]. However, systematic analysis of the changes in expression levels of CSE, CBS and 3MST with disease staging is currently unavailable.

Previously, we have exploited the 3MST pathway for the development of efficient and rapidly acting antidotes for cyanide toxicity [44]. Here 3MST enables transfer of a sulfur from 3-mercaptopyruvate to cyanide resulting in formation of non-toxic thiocyanate. Our approach involved synthesis of stable and more bioavailable prodrugs of 3-mercaptopyruvate. This program led to identification of sulfanegen as a promising lead candidate. Creation of various salt forms rendered this candidate sufficiently water-soluble for intramuscular administration [45]. The efficacy of sulfanegen has been demonstrated in various animal models and a comprehensive pharmacokinetic analysis is also available [46,47]. Intramuscular sulfanegen in rabbits has a plasma half-life of 114 min and plasma concentration-time plot fits a one-compartmental model with first order distribution and elimination [48]. Given the involvement of the H_2S pathway in neurodegenerative disorders, we examined sulfanegen for potential therapeutic effect against Alzheimer's disease. This approach overcomes the limitations of current H_2S donor therapeutics; specifically, stability and bioavailability. Provision of a prodrug of 3-mercaptopyruvate overcomes the involvement of CAT and presents a possibility for activation of the 3MST pathway. In turn, it also provides a tool for investigation of the role of 3MST in AD pathophysiology.

This report presents for the first time the evaluation of sulfanegen as a potential treatment for AD. We evaluated brain permeation, bioavailability of sulfanegen and its ability to counteract oxidative insults and $A\beta_{1\text{-}42}$ toxicity in cell culture. Mechanistic investigations aimed at elucidating the role of 3MST in H_2S release by sulfanegen were also conducted. Finally, *in vivo* efficacy studies were conducted in symptomatic transgenic AD mice and also in mice that were subjected to AD-like pathology induction through intracerebroventricular injection of $A\beta_{1\text{-}42}$. The results of these studies confirmed antioxidant and anti-inflammatory effects of sulfanegen treatment. Behavioral investigations demonstrated the potential of sulfanegen in restoring cognitive impairment observed in AD-like dementia. The results establish 3MST as a promising drug target and sulfanegen as a lead therapeutic for further drug development explorations against AD.

2. Materials and methods

Reagents. Sulforhodamine B (SRB), 2,2-diphenyl-1-picrylhydrazyl (DPPH), 7-azido-4-methylcoumarin (AzMC), 2′,7′-dichlorodihydrofluorescein diacetate (H_2DCFDA), I3MT3 and propargyl glycine (PAG) were purchased from Sigma (St. Louis, MO). Sulfanegen was synthesized by Sai Life Sciences Ltd. (India) using the synthetic procedures developed by us [44]. The compound was found to be >95% pure by elemental analysis (Supporting Information, Fig. S9) and was used in *in vitro* and *in vivo* experiments described in this study. The cell-counting kit-8 (CCK-8) was purchased from Dojindo Molecular Technologies (Rockville, MD). The $A\beta_{1\text{–}42}$ peptide for cytotoxicity assay was acquired from GenScript (Piscataway, NJ). A solution rich in monomeric $A\beta_{1\text{–}42}$ was prepared by treating the peptide with 1,1,1,3,3,3-hexafluoro-2-propanol (HFIP), followed by sonication, as described previously [49]. The cell culture medium (F12, MEM), fetal bovine serum (FBS), Gluta-MAX, MEM NEAA, and penicillin-streptomycin solution were purchased from GIBCO (Grand Island, NY). Gels for protein carbonyl assay (Bis-Tris SurePAGE™ gel 10%) were obtained from GenScript (Piscataway, NJ). The study utilized following primary antibodies: clone 4G8 anti-$A\beta_{17\text{–}24}$ mouse monoclonal antibody (BioLegend), clone 12F4 anti-$A\beta_{x\text{–}42}$ mouse monoclonal antibody (BioLegend), GFAP anti-rabbit polyclonal antibody (Dako, Glostrup Kommune, Denmark), Iba1 anti-rabbit polyclonal antibody (Wako, Japan), and TH (tyrosine hydroxylase) anti-rabbit polyclonal antibody (Millipore, Burlington, MA, USA). Goat anti-rabbit IgG HRP conjugated secondary antibody (no. 7074) was obtained from Cell Signaling Technology (Beverly, MA).

Cell Culture. SH-SY5Y, the human neuroblastoma cell line, was obtained from the American Type Culture Collection (ATCC) and maintained in MEM-F12 (1:1) supplemented with 15% FBS, 1% penicillin-streptomycin, 1% non-essential amino acids as mentioned in the ATCC protocol. Cells were maintained in a humidified incubator controlled at 37 °C with 5% CO_2.

Cytotoxicity Assays. Hydrogen peroxide toxicity (100 μM) in the absence and presence of sulfanegen was measured using a sulforhodamine B (SRB) assay. After incubation of cells for 24 h at 37 °C, the assay was terminated by addition of 10% trichloroacetic acid (TCA) with continued incubation for 1 h at 4 °C. This was followed by two washing steps before addition of the SRB solution (0.04% w/v SRB in 1% v/v acetic acid). The plate was incubated for additional 1 h at room temperature, washed with 1% acetic acid solution to remove unbound SRB and dried overnight. A 100 μL of Tris solution (10 mM tris base, pH = 10.5) was added to each well and absorbance was recorded at 510 nm.

For amyloid toxicity assay, the cells were allowed to reach 70% confluence before treating with a solution of $A\beta_{1\text{-}42}$ peptide (20 μM) in the absence and presence of varying concentrations of sulfanegen. Cytotoxicity was measured by following the instructions provided by the CCK-8 kit. Briefly, 10 μL of CCK-8 solution was added per well, followed by incubation for 3 h at 37 °C and the absorbance was read at 450 nm.

ROS Detection using DCFDA. SH-SY5Y cells (30,000/well) were treated with sulfanegen (200 μM) in the presence or absence of H_2O_2 (100 μM) for 8 h at 37 °C. A solution of DCFDA in serum-free media (1

μM) was added to each well and incubation was continued for additional 10 min. The cells were then washed twice with DPBS and fluorescence was measured at an excitation/emission wavelength of 485/535 nm. Images were captured using Cytation 1 fluorescence plate reader.

DPPH Assay. 2,2-diphenyl-1-picrylhydrazyl (DPPH) was used to measure the antioxidant activity of sulfanegen. Various concentrations of sulfanegen were incubated with DPPH (150 μM in 80% ethanol) for 30 min at room temperature and then the absorbance was measured at 517 nm [50].

Measurement of H_2S Liberation. Release of H_2S from sulfanegen was measured using a modified methylene blue assay described previously [51]. To 1% w/v agar was added a mixture of Zn acetate (45 mM) and NaOH (4.5 mM). The solution was then applied to the non-adherent surface of empty T-25 flasks and allowed to solidify. Cells were seeded at 1×10^6 cells/flask and incubated overnight at 37 °C. Treatment with sulfanegen (0–500 μM) continued for 6, 24 and 48 h, after which the media was removed and 2 mL N,*N*-dimethyl-*p*-phenylenediamine chloride was added to the agar layer. The resulting mixture was treated with 400 μL of ferrous chloride and incubated for 20 min. The absorbance at 670 nm was measured as an indicator of the amount of H_2S generated. Incubation with sodium hydrosulfide (NaSH) for 1 h was used as a positive control.

To study the role of 3MST in H_2S liberation by sulfanegen, a more sensitive fluorescent assay using 7-azido-4-methylcoumarin (AzMC) was used [52,53]. SH-SY5Y cells in a 96-well black plate were treated with a selective 3MST inhibitor, I3MT3 (500 μM) or an irreversible inhibitor of CSE, DL-propargyl glycine (PAG, 500 μM) for 6 h at 37 °C. The cells were then incubated with 10 μM of AzMC for 30 min in dark, followed by incubation for 1 h with various concentrations of sulfanegen and 3-mercaptopyruvate. Cells were then washed twice with PBS and fluorescence was measured at an excitation/emission wavelength of 340/445 nm.

Animals. Pharmacokinetic analysis of sulfanegen was conducted in 8 week old CF-1 mice purchased from Charles River (Wilmington, MA). Efficacy studies were conducted in C57BL/6 wild type mice (Charles River) injected intracerebroventricularly (i.c.v.) with $A\beta_{1\text{-}42}$ oligomeric solution and transgenic APPswe/PS1ΔE9 (APP/PS1) mice on C57BL/6 background (B6. Cg-Tg (APPswe, PSEN1dE9)85Dbo/Mmjax). For studies in transgenic mice, non-transgenic (NTG) littermates were used as controls. All animals were housed 4 per cage on a 12 h–12 h light-dark cycle, with access to food and water *ad libitum*. All experimental procedures and animal handling were executed in accordance with the national ethics guidelines, approved and complied with all protocol requirements at the University of Minnesota, Minneapolis, MN (IACUC). Mice were randomly assigned to study groups based on their age and genotype.

Bioavailability assessment and plasma to brain distribution study. For bioavailability study, 8-week-old male CF-1 mice after mice were administrated with sulfanegen by oral (50 mg/kg) and intravenous (10 mg/kg) route, and the blood was collected through the saphenous vein at 0.25, 0.5, 60, 120, 240, 360 min. For brain and plasma distribution, sulfanegen solution was injected into mouse peritoneum at 50 mg/kg dose. The animals were euthanized, and plasma and brain samples were collected at 0.5, 1, 2, 3 and 4 h after the drug administration.

For analysis of sulfanegen content, the brain tissues were homogenized by addition of 1:2 (w/v) of DPBS using a mechanical homogenizer. After de-proteinization using acetonitrile, plasma and brain homogenates were mixed with 5 mM ammonium formate solution containing monobromobimane (500 μM). The mixture was heated at 70 °C for 15 min and the samples were subjected to LC-MS/MS analysis. The samples were injected in an Agilent 1260 HPLC device coupled with an AB Sciex QTRAP 5500 mass spectrometer and separated using a Phenomenex Kinetex C18 column (50 mm × 2.1 mm, 2.6 μm) with a mobile phase of 5 mM ammonium formate in water (mobile phase A) and 0.1% formic acid in acetonitrile (mobile phase B) at a flow rate of 0.5 mL/min. The analytes were eluted with a gradient as follows: from 0 to 2 min, 3–70% B (v/v); from 2 to 3 min, 70% B (v/v); from 3 to 3.2 min, 70–3% B (v/v); from 3.2 to 6.5 min, 3% B (v/v). Samples were analyzed with an electrospray ionization source operated in the positive mode. The optimized source and gas parameters were as following: curtain gas, 25 psi; CAD gas, medium; ion spray voltage, 5000 V; temperature, 650 °C; gas 1, 60 psi; gas 2, 50 psi. Multiple reaction monitoring (MRM) was conducted by monitoring the following transition: m/z 311.0 → 223.1 (MRM1); 311.0 → 192.1 (MRM2). Non-compartmental analysis was conducted using Phoenix WinNonlin v8.1 (Certara USA, Inc., Princeton, NJ). Oral bioavailability (F%) was calculated using following formula: $F(\%) = (AUC_{po}/AUC_{iv}) \times (Dose_{iv}/Dose_{po})$. The brain to plasma ratio was calculated through the formula: $(AUC_{brain}/AUC_{plasma})$.

Sulfanegen Treatment in i.c.v. $A\beta_{1\text{-}42}$ injected non-transgenic and symptomatic APP/PS1 mice. Preparation of $A\beta_{1\text{-}42}$ peptide solution and i.c.v injections were conducted using protocols described previously [54]. Sulfanegen dissolved in saline was administered to 8–10 week old C57BL/6 mice at a dose of 50 and 100 mg/kg, once a day for 12 days. The $A\beta_{1\text{-}42}$ injection was performed on day 4 of the sulfanegen treatment. The mice were divided into three treatment groups (N = 8–10): (i) $A\beta_{1\text{-}42}$ only; (ii) $A\beta_{1\text{-}42}$ + sulfanegen (50 mg/kg); and (iii) $A\beta_{1\text{-}42}$ + sulfanegen (100 mg/kg). Age-matched animals with i.c.v. Saline injection were used as controls. Cognitive assessment by T-maze test was conducted on day 10 and 11 before euthanization of mice on day 12 for brain tissue collection.

Two cohorts of APP/PS1 mice, 7 and 12 months old, were administered with saline (N = 8) or intraperitoneal sulfanegen (75 mg/kg, N = 8). Treatment continued three times a week for 12 weeks, before the animals were sacrificed. T-maze behavioral assessments were conducted 10–11 weeks after initiation of sulfanegen treatment. We used equal numbers of male and female mice were used as much as possible.

Stereological Analysis of Aβ pathology and neuroinflammation. Quantitative analysis of Aβ pathology and neuroinflammation were performed using immunostained brain sections as previously described [55]. Briefly, frozen coronal sections (40 μm) were incubated with a primary antibody of interest, followed by detection using the ABC method (Vector Laboratories, Burlingame, CA, USA) with the chromogen, 3,3′-diaminobenzidine (DAB; Sigma Aldrich, St. Louis, MO, USA) for visualization.

Stereological analyses were performed using the Stereo Investigator software (Micro Bright Field; Colchester, VT). The extent of brain area covered by Aβ deposits (4G8 and 12F4), reactive astrocytes (GFAP), and microglia (CD68) within the regions of interest (ROI) was measured using the area fraction fractionator probe [55,56]. The ROIs were determined using The Mouse Brain Stereotaxic Coordinates [57] as the reference. Representative images are shown in the paper.

Stereological Analysis of noradrenergic afferents and neurons. The length of NAergic axons were estimated from TH stained forebrain sections using the stereological length estimation with spherical probes (Stereo Investigator; Micro Bright Field, Williston, VT, USA) as described previously [55,58]. Because of the regional variations in the densities of NAergic afferents, we focused our analysis on the selected subregions or ROIs (S1BF and dorsal hippocampus) for NAergic afferents. The total number of NAergic neurons in the LC was determined from TH stained brainstem sections using the optical fractionator as described previously [55,58]. For unbiased stereological analysis of neuronal size (area and volume), we used the nucleator probe of the Stereo Investigator as described previously [55,58].

$A\beta_{1\text{-}42}$ Sandwich ELISA Assay. Levels of soluble (PBS fractions) and insoluble Aβ (guanidine fractions) in cortical and hippocampal regions of 10 and 15 month cohorts were measured using sandwich ELISA as per the manufacturer's instructions (Invitrogen-KHB3441). Briefly, 50 μL of guanidine or PBS fractions of brain homogenates were added to a 96 well plate containing Aβ detection antibody and incubated for 3 h at room temperature. This was followed by incubations with 100 μL of anti-rabbit IgG HRP with brief intermediate washing steps. After addition of a 100 μL of chromogenic solution to each well, absorbance was measured at 450 nm using a Spectra Max M5 microplate reader. Levels

of $A\beta_{1-42}$ in each sample were normalized to protein content.

Quantification of protein carbonyls. Carbonylation of proteins were measured following the instructions provided by the Protein Carbonyl Assay kit from Abcam (ab178020). Briefly, the brain homogenates were first derivatized with DNPH solution and loaded onto a nitrocellulose membrane using a dot blot apparatus from Bio-Rad. The membrane was then blocked in Blotto non-fat milk solution for 1 h at room temperature and incubated with the primary antibody provided in the kit for 3 h at room temperature. Incubation with the secondary antibody and subsequent washing steps were followed by detection using western ECL substrate using ChemiDoc MP imaging system (Bio-Rad).

GSH ELISA Assay. Quantitation of reduced and oxidized GSH levels in the cortical and hippocampal brain regions of 10 and 15 month mice cohorts was performed using GSH ELISA kit (Cayman-703002). Briefly, deproteinated samples were subjected to enzymatic GSH recycling assay with glutathione reductase to calculate total and oxidized GSH content. Derivatization of the GSH thiol by 2-nitro-5-thiobenzoic acid (DTNB) and measurement of absorbance at 410 nm was used as an indicator of the GSH content.

TBARS Assay. Lipid peroxidation levels in mice brain were determined using TBARS assay kit (Cayman-10009055). Briefly, 10 μL of brain homogenate was incubated with SDS (10 μL) and a color reagent (400 μL) containing thiobarbituric acid for 1 h in boiling water. The vials were then immediately removed and placed in an ice bath for 10 min. The supernatants obtained after centrifugation of samples were read at excitation/emission wavelength of 530/550 nm.

Quantitation of inflammatory markers (TNF-α, IL-6). Brain cortical and hippocampus regions were analyzed for the levels of TNF-α (BMS607HS) and IL-6 (BMS603HS) using sandwich ELISA kits from Invitrogen as per the manufacturer's instructions. Measurements were recorded at 450 nm and the data was normalized to protein content of the sample.

Statistical analysis. All *in vitro* experiments were repeated for at least three times with each experimental condition and results are expressed as the mean ± SEM. Analysis of the *in vivo* experiments was conducted with N of at least 4/group. Statistical significance was determined by one-way ANOVA (analysis of variance) with Tukey's/Bonferroni's/Dunnett's multiple comparison test as appropriate using GraphPad Prism version 9, and values of $p \leq 0.05$ were considered statistically significant.

3. Results and discussion

Sulfanegen releases H_2S through the 3MST pathway and exhibits antioxidant property. The substrate of 3MST, 3-mercaptopyruvic acid, suffers from poor stability and bioavailability, limiting its use as a potential therapeutic. Developed as a prodrug of 3-mercaptopyruvate, sulfanegen is a suitable stable alternative [44]. Preclinical efficacy of sulfanegen as a cyanide antidote has been extensively evaluated

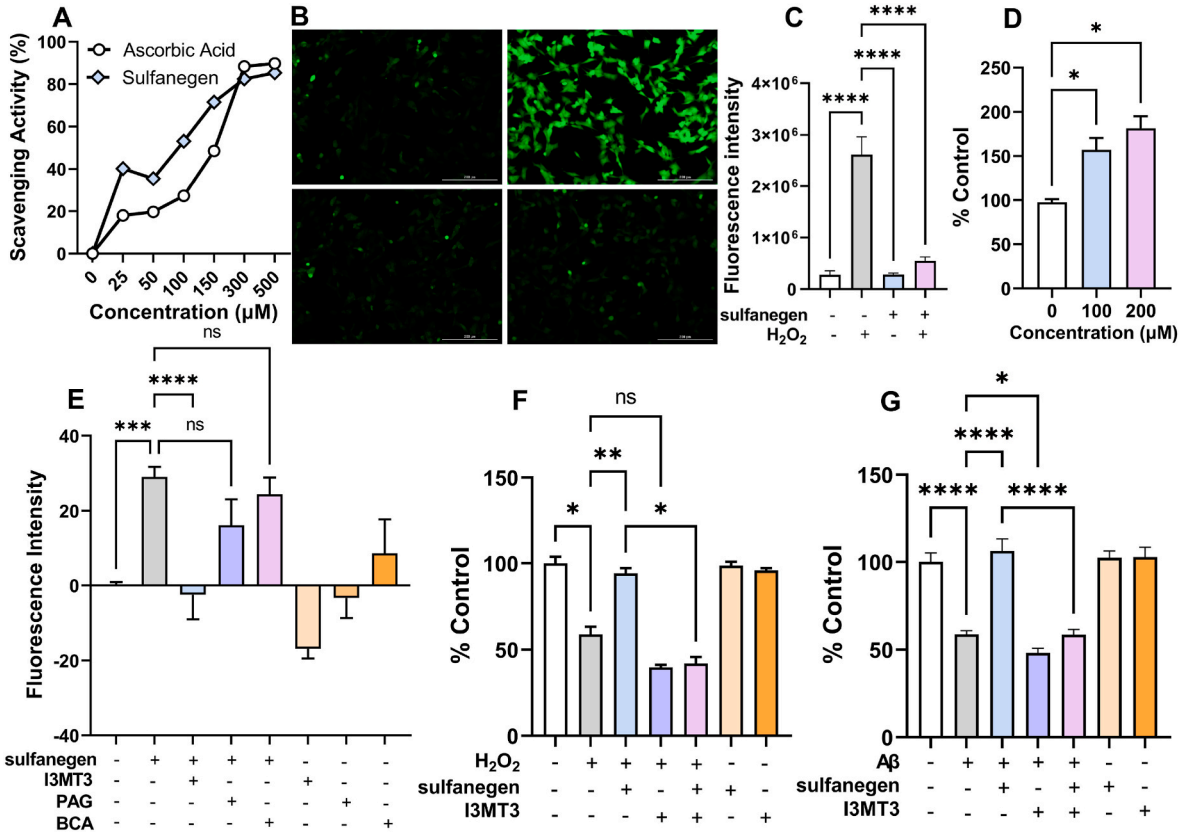

Fig. 1. Sulfanegen displays antioxidant property due to release of H_2S via 3MST pathway and mitigates peroxide and $A\beta_{1-42}$ cytotoxicity. (A) Radical scavenging property of sulfanegen was analyzed by a well-known DPPH assay as described in the methods section. (B) Cellular ROS generation was measured using DCFDA where cells were treated with H_2O_2 in the presence (top right) or absence of sulfanegen (bottom right) and images were taken after 8 h treatment. The left panel of images shows cells without H_2O_2 or sulfanegen exposure (top) and sulfanegen only (bottom controls). (C) Under similar conditions as B, fluorescence intensity was measured using a multimode plate reader. (D) Data represents dose dependent release of H_2S from sulfanegen. (E) H_2S release from sulfanegen was measured in the presence or absence of 3MST or CBS or CSE inhibitors as described in the methods section. (F) Protection of H_2O_2 cytotoxicity in the cells treated with sulfanegen in the presence or absence of 3MST inhibitor, I3MT3. (G) Cytotoxicity in the cells treated with $A\beta_{1-42}$ +/− sulfanegen in the presence or absence of I3MT3 after 24 h treatment. Statistical significance was assessed by a one-way ANOVA with Tukey's multiple comparison test. *$p < 0.05$, **$p < 0.01$, ***$p < 0.001$, ****$p < 0.0001$.

by us [46]; however, thorough mechanistic evaluation and application in CNS-related disorders have not been attempted. We thus tested the ability of sulfanegen to neutralize cellular oxidative stress and studied the role of 3MST in its antioxidant activity.

A standard DPPH assay, which relies on the ability of antioxidants to scavenge the DPPH radical, was used for measuring the antioxidant effect of sulfanegen. Incubation of varying concentrations (0–500 μM) of sulfanegen displayed dose-dependent radical scavenging activity, where the 500 μM concentration of compound displayed 85% scavenging activity. In comparison with the positive control ascorbic acid, sulfanegen displayed two-fold greater antioxidant capacity (IC_{50} of ascorbic acid = 141.4 μM, sulfanegen IC_{50} = 64.76 μM; Fig. 1A). These results were confirmed by evaluation of ROS quenching ability using the DCFDA probe (Fig. 1B–C). ROS production in cells was induced by exposure to H_2O_2 (100 μM) (Fig. 1B). Sulfanegen was able to abrogate ROS production by H_2O_2 as clearly seen by the reduction in DCFDA fluorescence in relation to cells treated with H_2O_2 alone (Fig. 1C).

Designed as a prodrug of 3-MP, sulfanegen is expected to exert its antioxidant effect by release of H_2S through 3MST pathway [44]. Liberation of H_2S after sulfanegen treatment was confirmed through a modified Zn-Acetate H_2S entrapment assay, which relies on zinc acetate-capture of released H_2S forming methylene blue dye for colorimetric quantitation. SH-SY5Y cells treated with sulfanegen for 6 h showed 57% and 81% increase in H_2S levels at 100 and 200 μM concentrations of sulfanegen respectively, when compared to vehicle control treated cells. In addition, we investigated time-dependent H_2S release in sulfanegen (200 μM) treated cells at 2, 6 and 24 h. The highest release of H_2S under these conditions was achieved at 6 h, which substantially decreased at 24 h, possibly due to practical limitations of this method to effectively trap the liberated H_2S (42, 72 and 27% increase in the H_2S release at 2, 6 and 24 h, respectively; Supporting Information, Fig. S1). Fig. 1D shows dose-dependent rise in the liberated H_2S in the cells treated with sulfanegen for 6 h. To confirm involvement of 3MST in sulfanegen-mediated H_2S release, this experiment was conducted in the presence of a selective 3MST inhibitor, I3MT3 [59]. Inhibitors of other endogenous H_2S releasing enzymes such as CBS and CSE were also employed to determine the contribution of 3MST toward the H_2S release caused by sulfanegen. A sensitive, H_2S-specific fluorescent probe, AzMC (7-azido-4-methylcoumarin), was employed for H_2S measurement. H_2S levels in the sulfanegen treated group (200 μM) showed a 30-fold increase over those in non-treated controls. The presence of I3MT3 (Fig. 1E) completely abrogated this effect. Incubations of sulfanegen with a CBS inhibitor, propargyl glycine (PAG) and a CSE inhibitor, β-cyanoalanine (BCA) caused no significant reduction in AzMC fluorescence intensity (an indicator of H_2S release), confirming that sulfanegen acts specifically through the 3MST pathway.

The release of H_2S and the innate reduction potential of sulfanegen is expected to provide relief from peroxide-induced cytotoxicity. Indeed, SH-SY5Y cells treated with H_2O_2 (100 μM) showed a 54% increase in cell death compared to control, which was completely prevented by sulfanegen (200 μM) pretreatment (Fig. 1F). Treatment with H_2S donors such as NaSH has also been found beneficial in Aβ-induced neurodegeneration with concomitant reduction in cellular oxidative stress [18–20,26,60]. The cytotoxicity of $A\beta_{1\text{-}42}$ is partly elicited through intracellular ROS formation and hence we evaluated sulfanegen's efficacy against Aβ-induced cell death. A significant loss of cell viability was caused by 20 μM $A\beta_{1\text{-}42}$ after 24 h incubation (40% cell death relative to cells exposed to scrambled Aβ peptide control, Fig. 1G), while co-treatment with sulfanegen (200 μM) rescued cells from Aβ-induced toxicity. To establish the relevance of 3MST in the protective effect of sulfanegen against peroxide and $A\beta_{1\text{-}42}$ toxicity, similar experiments were conducted in the presence of the 3MST inhibitor, I3MT3. The protective effect of sulfanegen was completely abolished by the 3MST inhibitor, confirming the biochemical mode of its action. A modest exacerbation of H_2O_2 and $A\beta_{1\text{-}42}$ cytotoxicity was observed in the presence of I3MT3 (20 and 10% rise over that of H_2O_2 and $A\beta_{1\text{-}42}$ alone, respectively). This results could stem from the necessity of the endogenous 3MST pathway for mitigating toxicities from oxidative insults. Cellular radical scavenging activity could arise from the liberated thiol in the form of 3-mercaptopyruvate, but more likely due to activation of antioxidant defense mechanisms and protein persulfidation caused by released H_2S [17]. Thus, enhancement of 3MST enzyme activity could be of benefit in disorders with underlying oxidative pathology.

In vivo brain distribution and pharmacokinetic evaluation of sulfanegen. A drug must attain pharmacologically relevant concentration in the target tissue(s) for it to be of practical utility in *in vivo* model systems. Sulfanegen successfully serves as an antidote for cyanide poisoning in large mammals (pigs) [46]. Studies investigating this effect, however, did not analyze CNS distribution of the compound. In this study, we measured the brain permeation of sulfanegen upon intraperitoneal injection at a 50 mg/kg dose. A C_{max} of 46 μM was noted in the brain 1 h post its administration and was found to be constant over the course of this experiment (Supporting Information, Fig. S2). The plasma concentration plummeted to the baseline within 2 h. Measurement of brain and plasma AUC over time, offered a brain and plasma ratio (B/P ratio) of 2.334, indicating that sulfanegen satisfactorily permeates into the brain to a therapeutically relevant extent. The relatively short plasma half-life of sulfanegen prevented estimation of free, protein unbound concentration of sulfanegen and calculation of the unbound partition coefficient (Kp, uu) [61], a true measure of the brain exposure of a compound.

In vivo pharmacokinetic analyses (Table 1) reconfirmed the short half-life of sulfanegen (2.11 h and 2.41 h after i. v. and p. o. administration, respectively). Overall exposure of sulfanegen appears to be similar upon i. v. or oral administration, as determined by the recorded AUC. Although cleared rapidly (2.30, and 8.29 L/h/kg for i. v. and oral dose, respectively), sulfanegen displayed a satisfactory volume of distribution. Overall, this resulted in a calculated oral bioavailability of 26.44%, suggesting that sulfanegen is a suitable candidate for further therapeutic investigations and future drug development efforts.

Sulfanegen improves cognitive function of mice treated intracerebroventricularly with $A\beta_{1\text{-}42}$ and mitigates neuroinflammation. The promising results from the *in vitro* studies compelled us to study the *in vivo* effects of sulfanegen treatment on AD pathology. Prior to extensive investigations of sulfanegen in a transgenic AD model that closely mimics human AD pathology, we evaluated its efficacy in an intracerebroventricularly (i.c.v)-injected $A\beta_{1\text{-}42}$ mouse model in non-transgenic mice. Cellular data indicated potential protective effect of sulfanegen against $A\beta_{1\text{-}42}$ neurotoxicity (Fig. 1). The i.c.v.-injected Aβ model has an advantage over other acute AD models such as chemically induced AD model in that it is produced by AD-specific pathogenic insult, and has cost and time benefits over the transgenic AD models [54]. After pretreatment with sulfanegen at 50 and 100 mg/kg, $A\beta_{1\text{-}42}$ oligomeric solution was injected on day 4 (Fig. 2A). The choice of

Table 1
Non-compartmental pharmacokinetic parameters of sulfanegen after intravenous and oral administration (N = 4/group).

Parameters	i.v. (10 mg/kg)	*p.o.* (50 mg/kg)	*Bioavailability*
$t_{1/2}$ (h)	2.1122	2.4065	26.44%
T_{max} (h)	0.25	0.5	
C_{max} (μmol/L)	8.66	16.4	
AUC_{0-t} (h·μmol/L)	13.58	17.95	
$AUC_{0-\infty}$ (h·μmol/L)	18.03	25.07	
MRT_{0-t} (h)	1.5523	1.4036	
V (L/kg)	7.0309	28.8056	
CL (L/h/kg)	2.3073	8.297	

$t_{1/2}$, terminal half-life. **T_{max},** time to reach maximum plasma concentration. **C_{max},** maximum plasma concentration. **AUC_{0-t},** area under the concentration-time curve from the time of dosing to the last quantifiable time point. **$AUC_{0-\infty}$,** area under the concentration-time curve extrapolated from the time of dosing to infinity. **MRT**, mean residence time. **V**, volume of distribution. **CL**, clearance.

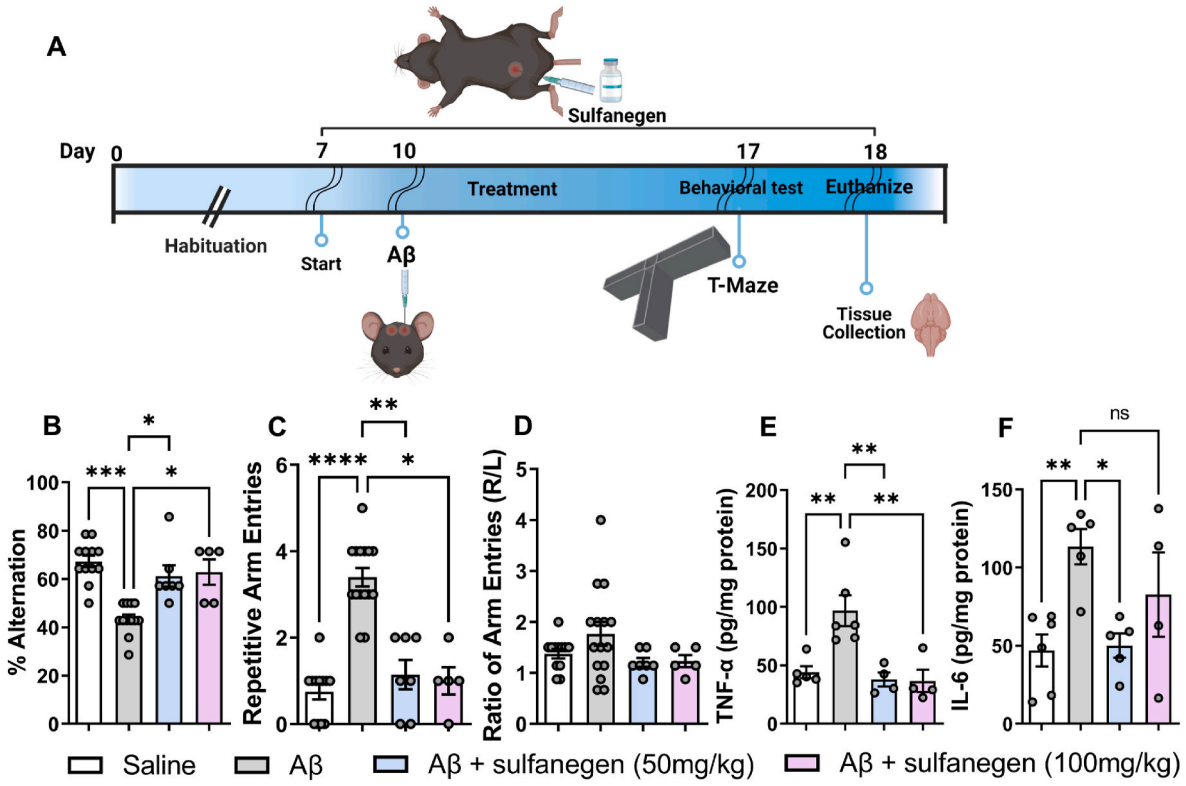

Fig. 2. Sulfanegen administration shows improved cognitive behavior and inflammatory pathology in the brain tissues of mice injected intracerebroventricularly with oligomeric $A\beta_{1\text{-}42}$ solution. (A) Time course of the i.c.v. Aβ-model, created using BioRender.com. (B) Cognitive assessment was conducted using T-maze test on day 10 after $A\beta_{1\text{-}42}$ injection. A significant reduction in the alternation behavior observed in $A\beta_{1\text{-}42}$ only mice was improved in sulfanegen treated mice. Similarly, significant improvement in number of repetitive arm entries was observed in the compound treated group (C). There was no innate spatial bias displayed by these mice as evident from the ration of left and right arm entries (D). Neuroinflammatory markers such as TNF-α (E) and IL-6 (F) were elevated in $A\beta_{1\text{-}42}$-only group and sulfanegen treatment rescued against this inflammatory phenotype in this mouse model. Statistical significance was assessed by a one-way ANOVA with Tukey's multiple comparison test. *p < 0.05, * *p < 0.01, ***p < 0.001, ****p < 0.0001.

sulfanegen dose was based on the *in vivo* biodistribution data to achieve therapeutically relevant concentrations in the brain. Cognitive behavioral analysis was conducted by the T-maze test at the end of compound treatment period. This test which depends on the proclivity of mice to explore novel environments, is able to detect dysfunction in the hippocampus, prefrontal cortex regions, which typically results in spatial working memory deficits in $A\beta_{1\text{-}42}$ injected mice. Such cognitive impairment was evident from the reduced alternation behavior in $A\beta_{1\text{-}42}$-only injected mice; specifically, a 32% reduction in alternation rate was observed in the i.c.v. $A\beta_{1\text{-}42}$ treated group compared to the saline treated controls (Fig. 2B). This aberrant behavior was restored to control levels in sulfanegen treated groups at both of the doses tested. Similarly, i.c.v injection of $A\beta_{1\text{-}42}$ caused a 3-fold increase in the number of repetitive arm entries (Fig. 2C), while this was attenuated to vehicle controls levels in both compound treated groups. The ratio of left and right arm entries of the T-maze was not different among the treatment groups (Fig. 2D), indicative of the absence of spatial bias in these mice. Additionally, no motor dysfunction or physical incapacitation was observed in the mice based on similar total time taken to complete the test. The higher dose of sulfanegen (100 mg/kg) caused toxicity in the mice as assessed by greater than 10% loss in the body weight and a mortality rate of 22%.

Although the i.c.v. $A\beta_{1\text{-}42}$ model does not reproduce Aβ plaque pathology of human AD brain, it reliably recapitulates neuroinflammatory consequences of $A\beta_{1\text{-}42}$ toxicity. We evaluated brain expression of pro-neuroinflammatory cytokines such as TNF-α (Fig. 2E) and IL-6 (Fig. 2F) in these mice. In accordance with the behavioral data, $A\beta_{1\text{-}42}$-only treated mice displayed significant elevation in the expression levels of these markers. The lower dose sulfanegen group (50 mg/kg) mitigated the inflammatory damage, in that it reduced the expression of TNF-α and IL-6 to the levels observed in vehicle control mice. The higher dose of sulfanegen (100 mg/kg) did reduce these inflammatory markers, but less effectively. This could potentially be attributed to toxicity of the compound itself at this higher dose.

Transgenic mice treated with sulfanegen display improved cognitive behavior and lower brain Aβ burden. Limited clinical success of potential AD therapeutics in the past warrants testing of emerging therapeutics in multiple animal models of AD to truly model clinical AD pathology. Transgenic AD models closely replicate the pathology observed in human AD and are widely utilized for preclinical testing of AD therapies. We utilized the APP/PS1 mouse model of AD for further evaluation of sulfanegen's efficacy. To approximate the clinical use, treatment was initiated in aged mice with established AD pathology. Two cohorts of APP/PS1 mice aged 7 and 12 months were treated intraperitoneally with 75 mg/kg sulfanegen for 12 weeks. This choice of the dose stemmed from the finding in the acute AD model that the 100 mg/kg was toxic, but both the 50 and 100 mg/kg showed mitigation of neuroinflammatory pathology. We utilized the T-maze cognitive test for assessment of spatial working memory impairment 8 and 12 weeks after treatment initiation. A significantly lower alternation rate and higher repetitive behavior, similar to the behavior observed in the i.c.v. $A\beta_{1\text{-}42}$ injected animals, was displayed by the saline treated APP/PS1 mice at the end of 12-week treatment period (Fig. 3A–C). Sulfanegen treatment displayed dramatic improvement in percentage alternation (APP/PS1/Saline: APP/PS1/Sulfanegen: WT/Saline; 48 ± 6.99%, 65 ± 2.9%, 73 ± 5.3%, respectively; Fig. 3A) and reduced number of repetitive arm entries (APP/PS1/Saline: APP/PS1/Sulfanegen: WT/Saline; 3.6 ± 0.5, 1.2 ± 0.4, 0.8 ± 0.3, respectively; Fig. 3B), both comparable to the levels in

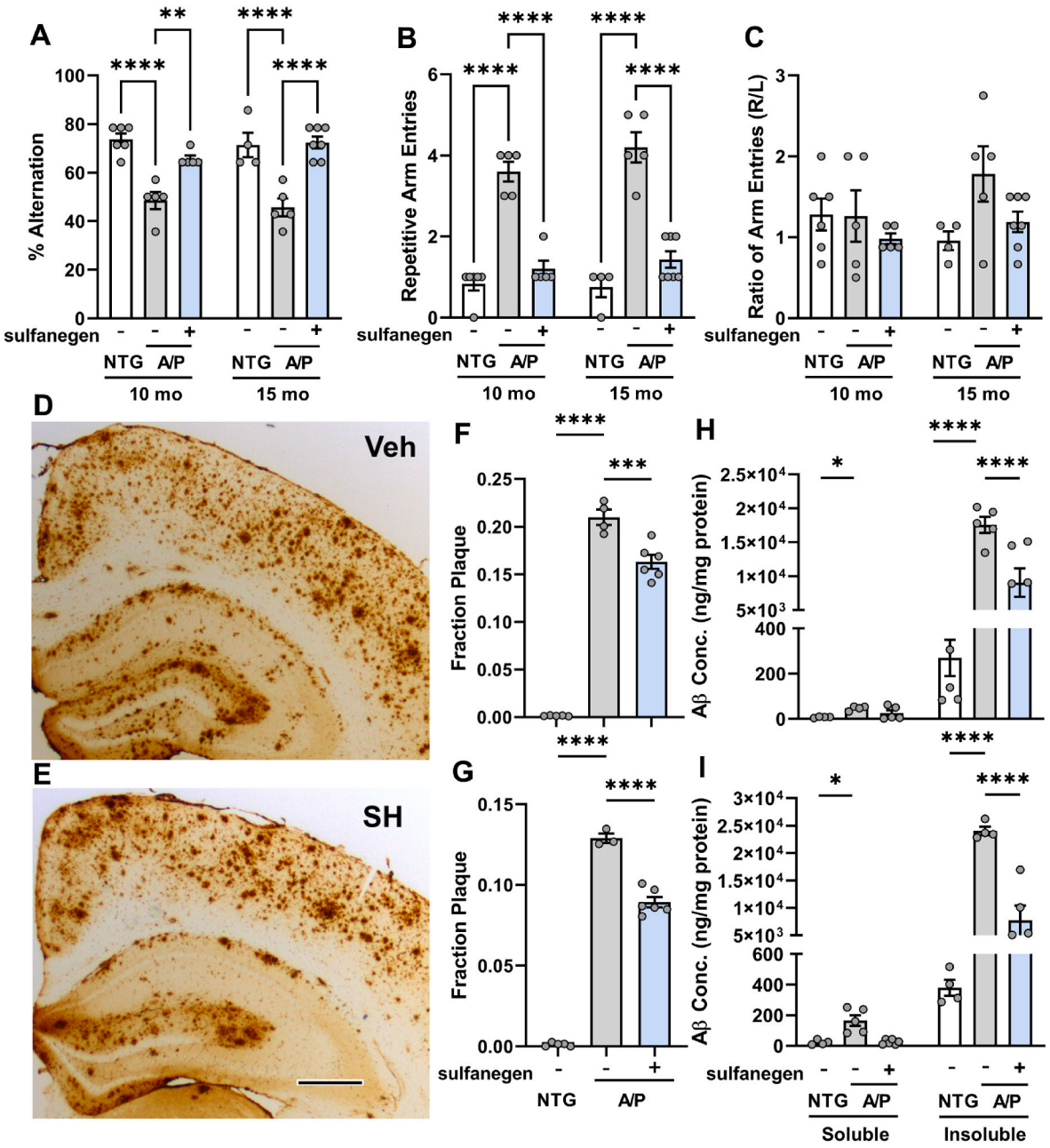

Fig. 3. Sulfanegen administration improves cognitive behavior and reduced Aβ plaque burden in APP/PS1 mice. (A–C) Cognitive assessment of 10 and 15 mo old APP/PS1 cohorts was conducted using the T-maze test. Percent alternation (A) and repetitive arm entries (B) showed significant improvement in the sulfanegen treated mice compared to transgenic vehicle controls. No spatial bias (C) was observed as deemed by ration of arm entries. (D–E) Representative images of immunohistochemical detection of amyloid plaques using 4G8 antibody in cortex and hippocampal regions. Quantitation of the plaque-covered area in cortex (F) and hippocampus (G) regions of the 15 mo old cohort displayed significant reduction in compound treated group. (H–I) ELISA-based quantitation of Aβ levels showed significant reduction in the insoluble Aβ levels in the cortex (H) and hippocampus (I) of 15 mo old cohort. Statistical significance was assessed by a one-way ANOVA with Tukey's multiple comparison test. **p < 0.01, ***p < 0.001, ****p < 0.0001.

non-transgenic controls as shown in Fig. 3. Similar improvement in cognitive behavior was also observed in the 15-month cohort (Fig. 3A–C), indicating efficacy of sulfanegen treatment even during advanced stages of AD. The test controls for determining spatial bias and motor dysfunction failed to detect significant changes among different treatment groups in both cohorts, as determined by the ratio of arm entries (Fig. 3C) and total time taken (data not shown) to complete the test. The results of cognitive assessment at 8 weeks after treatment initiations are included in the Supporting Information (Fig. S3) and the improvement in cognitive function was apparent at this early time point as well. This cognitive behavioral data suggests potential therapeutic utility of sulfanegen in advanced stages of the disease, where most of the available treatment have shown limited success.

One of the pathological hallmarks of AD is deposition of $A\beta_{1\text{-}42}$ plaques, which initiate changes leading to cognitive dysfunction [62–64]. Significant increase in Aβ levels and Aβ plaque deposition is observed in the cerebral cortex and hippocampus of APP/PS1 mice [55]. Supplementation with hydrogen sulfide is known to result in enhanced Aβ clearance and significant reduction in Aβ plaque burden, thereby improving motor and cognitive functions in an AD mouse model [65]. Being an activator of endogenous H_2S pathway through restoration of 3MST activity coupled with improved cognitive behavior presented by

sulfanegen-treated mice, its effect on $A\beta_{1-42}$ levels was evaluated next. As Aβ pathology begins as early as 6 months in the APP/PS1 mice [66,67], notable deposits of $A\beta_{1-42}$ plaques were visible in the cortex and hippocampal regions of 10 and 15 mo old cohorts (Fig. 3D–E). Transgenic mice treated with sulfanegen in the 15 mo old cohort (Fig. 3E) displayed modest, but significant reductions in the 12F4 ($A\beta_{x-42}$) staining of Aβ plaques in these regions. Quantitative analysis of cortex and hippocampal regions confirmed significant reduction in Aβ plaque burden in compound treated groups compared to age-matched vehicle treated transgenic controls (Fig. 4F–G). Concomitantly, we confirmed these stereological findings through independent ELISA analysis of $A\beta_{1-42}$ levels in these brain regions of the 15 mo old cohort (Fig. 4H–I). The levels of insoluble $A\beta_{1-42}$ (guanidine fraction) were significantly reduced in this cohort of mice treated with sulfanegen when compared to saline-treated transgenic controls. Similar effect of sulfanegen was observed on the levels of insoluble $A\beta_{1-42}$ in the 10 mo old cohort in both cortex and hippocampal regions (Supporting Information, Fig. S4). Effect of treatment on soluble $A\beta_{1-42}$ levels (PBS soluble fraction) was also observable in both age-group cohorts, but failed to reach statistical significance. With soluble $A\beta_{1-42}$ oligomers being increasingly recognized as the neurotoxic species, this effect of sulfanegen is valuable. Thus, these results show that the Aβ deposition in the form of insoluble Aβ increased with age in the APP/PS1 mice and the levels of the later were attenuated by sulfanegen treatment even in symptomatic APP/PS1 mice irrespective of age.

Mitigation of oxidative stress in aged APP/PS1 after sulfanegen treatment. Compromised endogenous antioxidant defense and increased oxidative stress has been reported by us [55] and others in the APP/PS1 model. Hydrogen sulfide is known to restore cellular GSH stores and diminish oxidative stress [18] resulting from amyloid pathology in AD models [60,68,69]. We studied the effect of sulfanegen treatment on the levels of GSH, specifically the ratio of reduced to oxidized GSH (GSH/GSSG) as a surrogate for the redox potential of the brain tissue (Fig. 4A). In both, the 10 and 15 mo old cohorts, the mean ratio of GSH/GSSG was two-fold lower in the saline treated transgenic mice relative to the age-matched wild type controls (NTG/Saline) as shown in Fig. 4A, indicating increased oxidative stress and decreased antioxidant potential. Treatment with sulfanegen rectified the GSH/GSSG ratio in both age groups of mice, thus correcting GSH deficits and alleviating the oxidative stress. This data corresponds with higher levels of reduced GSH found in sulfanegen treated mice, comparable to the levels found in age-matched wild type mice (Supporting Information, Fig. S5).

In addition to the effect on GSH levels, we examined the brain tissue for other indicators of oxidative stress. Reactive oxygen species damage a host of other macromolecules. Oxidation of lipids, for instance, forms hydroperoxides that in turn produce reactive intermediates such as malondialdehydes. Quantitation of lipid peroxidation levels using the thiobarbituric acid reactive substances (TBARS) assay showed significantly increased MDA levels in the brain homogenates of aged transgenic mice over those found in wild type mice (Fig. 4B). These levels were normalized with sulfanegen treatment in both the cohorts. Another consequence of oxidative damage is protein modification through carbonylation. Consistent with the results of GSH and lipid peroxide levels, increased protein carbonylation was found in the transgenic mice (Fig. 4C–D). Dot blot analysis of brain homogenates was conducted using the protein carbonyl (anti-DNP) antibody. Sulfanegen treatment reversed these oxidative modifications to wild type control levels.

Aside from oxidative pathology, chronic brain inflammation occurs in AD mice at early stages of the disease. Treatment with antioxidants such as H_2S donors is known to alleviate such inflammatory pathology. We examined the effect of sulfanegen on the brain levels of pro-inflammatory markers TNF-α and IL-6 in the transgenic mice (Fig. 4E–F). The cortex (Fig. 4E–F) and hippocampal regions (Supporting information, Fig. S6) in both ages of transgenic mice displayed elevated expression of TNF-α (Fig. 4E) and IL-6 (Fig. 4F), indicating ongoing inflammatory pathology in these mice. These markers were markedly reduced in the sulfanegen treated mice. Sulfanegen, potentially through restoration of 3MST function and possibly also through direct chemical ROS reduction, appears to be capable of mitigating these pathologies and could slow down or halt the progression of this disease.

Sulfanegen reduces astrocyte and microglia reactivity in symptomatic APP/PS1 mice. In addition to the levels of inflammatory cytokines such as TNF-α and IL-6, we evaluated the levels of reactive astrocytes by staining for glial fibrillary acidic protein (GFAP). A significant increase in GFAP staining was observed in the cortex and hippocampus regions of both 10-mo and 15-mo-old APP/PS1 mice (15 mo cohort, Fig. 5A–E; 10 mo cohort, Supporting Information, Fig. S7, respectively), which corresponded with Aβ plaque deposition in these brain regions (Fig. 3F–G). Sulfanegen-treatment resulted in a modest, but significant reduction in the cortical GFAP in both of the age groups of APP/PS1 mice (Fig. 5C–E; Supporting Information, Fig. S7). Reduced GFAP staining was also observed in the hippocampal region of sulfanegen-treated mice.

To selectively analyze activated microglia, we stained brain tissue sections for an activated microglia marker, CD68. In the 10 and 15 mo-old APP/PS1 mice, the CD68 staining is prominent, while negligible CD68 staining is seen in NTG littermates (Fig. 5F–H). Consistent with the GFAP staining, sulfanegen treatment resulted in modest reduction in the activated microglia in the cortex of the APP/PS1 mice (Fig. 5I). Hippocampal CD68 expression offered similar trend, with significant reduction in CD68 levels resulting in sulfanegen treated mice (Fig. 5J). Taken together, these data suggest that sulfanegen treatment induces protective mechanisms including anti-inflammatory and antioxidant responses that serve to reduce pathological Aβ load. Importantly, this phenomenon is seen even at late, symptomatic stages in this AD mouse model.

Sulfanegen protects against progressive noradrenergic neurodegeneration in APP/PS1 mice. It is widely recognized that the locus coeruleus (LC) in the brainstem is one of the earliest sites of neurofibrillary tangles formation in AD. Patients with both idiopathic and familial forms of AD exhibit early neuronal loss in the LC affecting its function. The LC is the primary source of norepinephrine, a major neurotransmitter involved in attention, memory and thus neurodegeneration in this region has detrimental effect on cognitive function [70,71]. The severity of neuronal loss in the LC often correlates with the severity AD symptoms. Previously, we have reported that the degeneration of the LC neurons seen in human AD is correctly modeled in APP/PS1 mice [58]. We hence examined the effect of sulfanegen on progressive degeneration of noradrenergic neurotransmitter system in APP/PS1 mice. Consistent with the lack of Aβ pathology in NTG mice, noradrenergic afferents and axons of saline-treated NTG mice did not reveal any significant observation (Fig. 6A). However, analysis of the cortical NAergic afferents in APP/PS1 mice shows significant loss of TH+ fibers in 10 mo old APP/PS1 mice that progresses to greater loss in 15 mo old APP/PS1 mice (Fig. 6B). Significantly, sulfanegen treatment rescued the cortical TH+ axon loss even when the treatment started after the onset of neurodegeneration (Fig. 6C). In particular, the fact that TH+ axon density in sulfanegen-treated APP/PS1 mice at 15 months of age is comparable to that seen in 10 mo old APP/PS1 mice indicate that sulfanegen was able to completely stop the progression of further neurodegeneration.

We previously showed that Aβ deposition leads to initial loss of noradrenergic axons followed by atrophy of cell bodies and finally the loss of TH+ neurons in the LC [58]. This loss is attenuated by supplementation with a metabolically stable GSH analogue [55]. Thus, we examined whether sulfanegen treatment also reversed the progressive neuronal atrophy and loss in APP/PS1 animals. Consistent with previous study showing that the loss of neurons occurs after 12 months of age in APP/PS1 mice, there was no significant loss of LC neurons at 10 mo APP/PS1 mice compared to NTG controls. However, the loss of cortical afferents at 15 mo APP/PS1 mice (Fig. 6F) is reflected by the decrease in

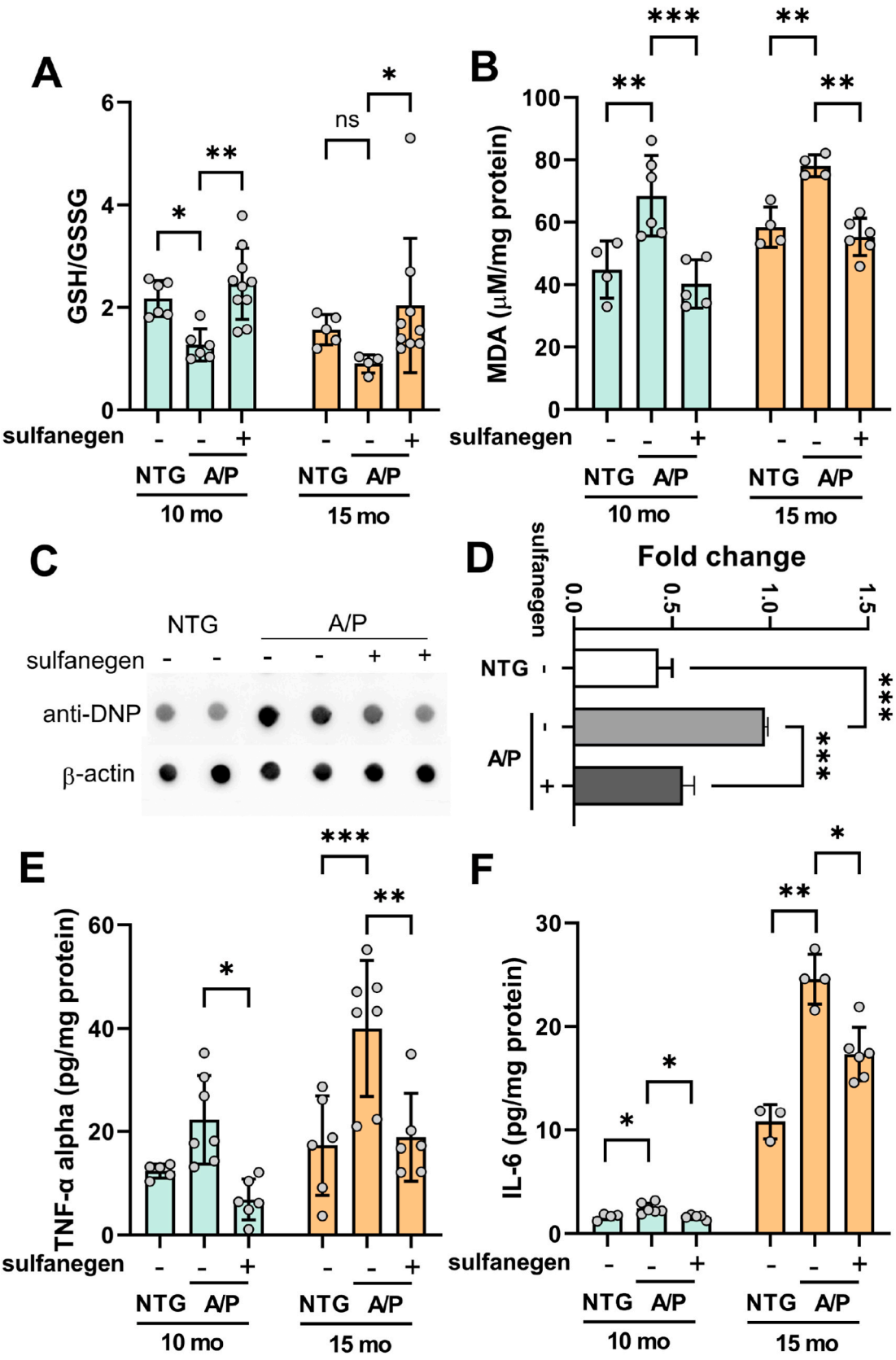

Fig. 4. Administration of sulfanegen in APP/PS1 mice reverses oxidative stress and reduces inflammation. (A–D) Overall oxidative stress was assessed by measurement of hallmark markers such as redox ratio (GSH:GSSG ratio, A), lipid peroxidation by thiobarbituric acid reactive substance, malondialdehyde (B), protein carbonyls using western blots with anti-DNPH antibody (C) in the cortex. Quantitation of dot blot in C is displayed in D. Assessment of inflammatory markers such as TNF-α (E) and IL-6 (F) was conducted in 10 and 15 mo old cohorts. Significant reduction in the levels of oxidative and inflammatory markers was observed in sulfanegen treated groups. Statistical significance was assessed by a one-way ANOVA with Dunnett's multiple comparison test. *$p < 0.05$, **$p < 0.01$, ** *$p < 0.001$.

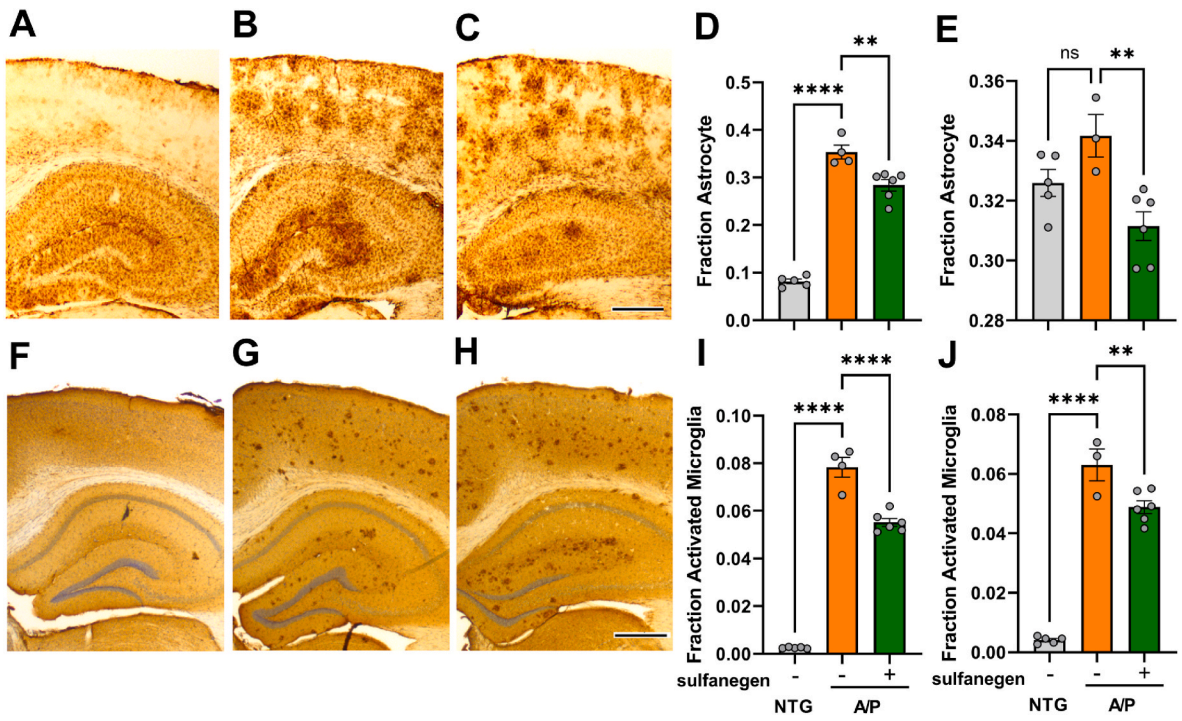

Fig. 5. Sulfanegen treatment reduces reactive astrogliosis and microglial reactivity in symptomatic 10- and 15-mo APP/PS1 mice. (A–C) Representative images of reactive astrocytes visualized by GFAP antibody in cortex and dentate gyrus of 15 mo NTG (A) and APP/PS1 mice treated with vehicle (B) or sulfanegen (C). Scale bar, 100 μm. (D–E) Quantification of GFAP staining in S1BF (E) and hippocampus (E) of the 15 mo old cohort. (F–H) Representative images of microglia visualized using CD68 antibody in cortex and hippocampal regions of 15 mo NTG (F) and vehicle (G) or sulfanegen (H) treated APP/PS1 mice. Scale bar, 100 μm. (I–J) Quantification of CD68 staining in S1BF (I) and hippocampus (J) of the 15 mo old cohort. Data are presented as mean ± S.E.M. For comparisons between NTG, saline-, and sulfanegen-treated APP/PS1 groups, a one-way ANOVA with Tukey's post-hoc test was used for data analysis. $^{**}p < 0.01$, $^{****}p < 0.001$.

neuronal volumes of TH+ cells in the LC (Fig. 6E–G). Sulfanegen treatment had significant impact on the overall TH+ neuronal counts in the 15 mo-old APP/PS1 mice (Fig. 6G–H). Significantly, in the 15 mo old APP/PS1 mice treated with sulfanegen from 12 months of age, progressive loss of TH+ neurons in LC was thus completely abated. In the 15 mo APP/PS1 mice, there was a significant reduction in neuronal volumes in LC (Fig. 6J and L). The neuronal volumes were significantly higher in the sulfanegen treated group (Fig. 6K-L). These data demonstrate the capacity of continuous sulfanegen treatment, delivered intraperitoneally, to protect against NAergic neurotransmitter network even in the late stage of AD pathology and symptoms. Robust neuroprotection of LC neurites and neurons despite the modest effects observed on the primary neuropathology, such as amyloid pathology and microglial activation (Figs. 3 and 5), suggest that sulfanegen may be acting downstream of amyloid pathology. Furthermore, these results could indicate that optimization of dose and/or treatment regimen may be necessary, along with the development of analogs with improved plasm half-life. Our results concur with other reports that suggest a neuroprotective role of H_2S donors in animal models of AD [25,72].

Sulfanegen restores impaired 3MST function in symptomatic APP/PS1 mice. Given the importance of hydrogen sulfide in brain homeostasis, the role of 3MST pathway cannot be overlooked (*30*). It is however unknown whether expression and/or function of 3MST is affected by the underlying pathology in the AD brain. The role of 3MST in the CNS has been very little elucidated, while none addressing specifically its involvement in the neurodegeneration in Alzheimer's disease [43,73]. We examined for the first time, the impact of progressive disease pathology in symptomatic APP/PS1 mice on the expression of 3MST. The expression of 3MST appeared unaffected in the cortex of transgenic AD brains in the 15 mo old cohort (Fig. 7A) as well as in the 10 mo old cohort. Clearly, the protein expression is not compromised by the neuropathology present at the advanced disease stage. We thus hypothesized that the increased oxidative stress and reduced GSH levels may alter 3MST function in the disease brain by limiting the availability of this enzyme's substrate, 3-mercaptopyruvate. Consequently, we measured the level of 3-mercaptopyruvic acid in both i.c.v and transgenic mouse brain homogenates using LC-MS/MS. Indeed, significant reduction in 3-MP concentration was observed in the i.c.v. Aβ1-42-treated (Supporting Information, Fig. S8) and transgenic APP/PS1 mice (Fig. 7B). Age dependent decrease in 3-MP level was also noted in the APP/PS1 mice (10 mo APP/PS1/saline: 15 mo APP/PS1 mice; 0.27 ± 0.10, 0.22 ± 0.01 μmol/mg protein), as well as in wild type mice (10 mo - NTG Saline: 15 mo NTG saline; 0.54 ± 0.03; 0.29 ± 0.01 μmol/mg protein). We next examined the effect of reduced 3-MP levels on endogenous 3MST activity in both acute and transgenic AD mice. Compromised 3MST function was evident in i.c.v. Aβ-only treated animals compared to vehicle control group (saline: Aβ; 322.5 ± 94.6, 122.9 ± 64.1, relative fluorescence/mg protein; Supporting Information, Fig. S8). Supplementation with sulfanegen restored the enzyme function (Aβ + sulfanegen 50 mg/kg: Aβ + sulfanegen 100 mg/kg; 365.8 ± 74.8, 387.3 ± 63.2 relative fluorescence/mg protein; Supporting Information, Fig. S8). Similarly, both cohorts of transgenic mice displayed practically undetectable enzymatic activity, which was restored to wild type controls levels upon chronic sulfanegen treatment in 10 mo and 15 mo old cohorts. Relative differences in the extent of 3MST function restoration could partly be explained by increased oxidative stress in the 15 mo old cohort in relation to 10 mo APP/PS1 mice, requiring portion of the available sulfanegen for neutralization of ROS and thus a lower amount of sulfanegen would be available for restoration of enzymatic function. Rigorous dose-response studies, leading to thorough treatment regimen optimization may overcome this limitation. These results, for the first time, provide data in support of compromised 3MST function and not its expression, in the symptomatic APP/PS1 mice. Until now, the knowledge about the influence of 3MST on AD is sparse, perhaps due to unavailability of stable chemical tools to probe its function. Development of sulfanegen has paved the way toward understanding the role of this

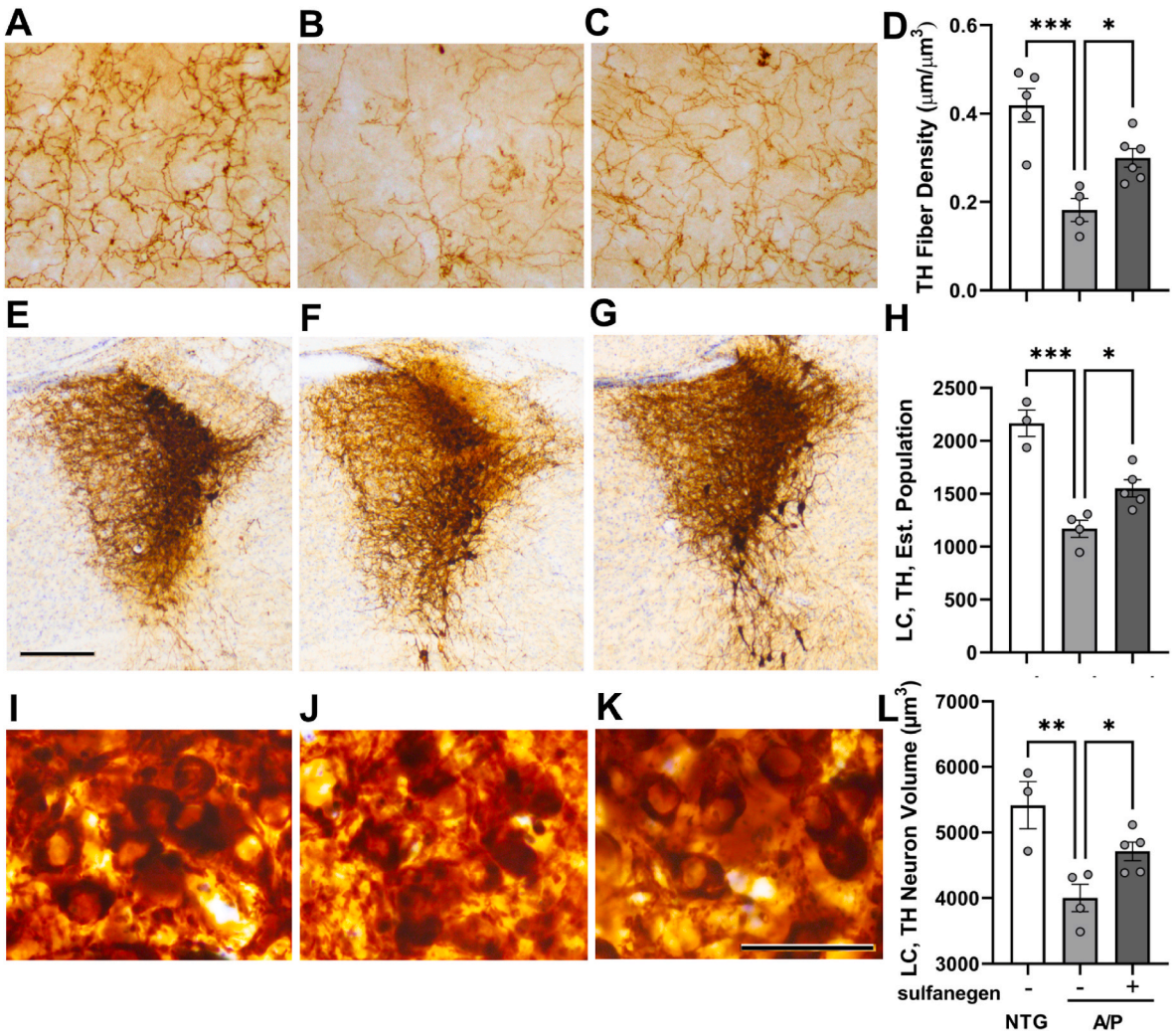

Fig. 6. Sulfanegen treatment after the onset of AD-like neuropathology halts the progressive degeneration of the NAergic cortical afferent axons in symptomatic 15 mo APP/PS1 mice. (A–C) Representative images of TH+ axonal projections in S1BF of the 15 mo old cohort; (A) NTG, (B) APP/PS1 vehicle and (C) APP/PS1 sulfanegen. Scale bar, 20 μm. (D) Quantification of TH+ axonal density in 15 mo old cohort. Density estimation (μm/μm^3) was determined using the Spherical probe on Stereo Investigator Software. (E–G) Representative images of TH+ neurons of the LC in both the 15 mo NTG (E) and vehicle (F) or sulfanegen (G) treated APP/PS1 mice. Scale bar, 100 μm. (H) Quantification of TH+ neurons in the LC in 15 mo old cohort. Estimated population was determined by the Optical Fractionator probe on Stereo Investigator software. (I–K) Higher magnification images of the TH+ neurons in the LC of 15 mo old cohort comprising NTG (I) and vehicle (J) or sulfanegen (K) treated APP/PS1 groups. Scale bar, 50 μm. (L) Quantification of the TH+ neuronal volume in 15 mo old cohort. Data are presented as mean ± S.E.M. A one-way ANOVA with Tukey's post-hoc test was used for statistical comparisons (b). *$p < 0.05$, **$p < 0.01$, ***$p < 0.005$.

biochemical pathway in AD. Whether reduced 3MST function is a consequence or a cause for AD progression, still needs to be determined. However, this study serves to establish the importance of 3MST in the molecular pathophysiology of AD.

4. Conclusion

In summary, the symptomatic APP/PS1 mice replicated multiple aspects of human AD including the increased oxidative stress, neuroinflammation and progressive neurodegeneration. Such underlying biochemical changes caused limited alternations to the expression of 3MST enzyme, however function of the enzyme was compromised due to limited supply of the substrate 3-MP. Sulfanegen substituted for 3-MP in the 3MST enzymatic reaction *in vivo* and restored the enzymatic function in the brain. The fact that supplementation with sulfanegen rectifies all of the pathological parameters in aged APP/PS1 models suggests that reduced brain GSH and consequently reduced 3-MP levels, contribute toward molecular pathology stemming from amyloidopathy — particularly the progressive degeneration of LC neurons. Limited mechanistic scope of this study warrants further investigation into pathways intricately linked to neuroprotective activity of H_2S. Detailed analysis of protein persulfidation levels, expression and function of key proteins involved in AD pathogenesis, modulation of antioxidant and anti-inflammatory defense systems by sulfanegen will be explored. To our knowledge, this is the first account of the relevance of 3MST to neurodegeneration and cognitive impairment observed in AD. The data presented support supplementation of 3MST as a viable approach to tackle the molecular pathology of AD. Consequently, this study establishes sulfanegen as a promising drug candidate for a true disease-modifying intervention into the ravages of Alzheimer's disease.

Funding

This research was supported by the National Institutes of Health Grants to SSM (R01-AG062469) and MKL (RF1-AG062135, R01-NS108686) and by funding from the Center for Drug Design (CDD), University of Minnesota.

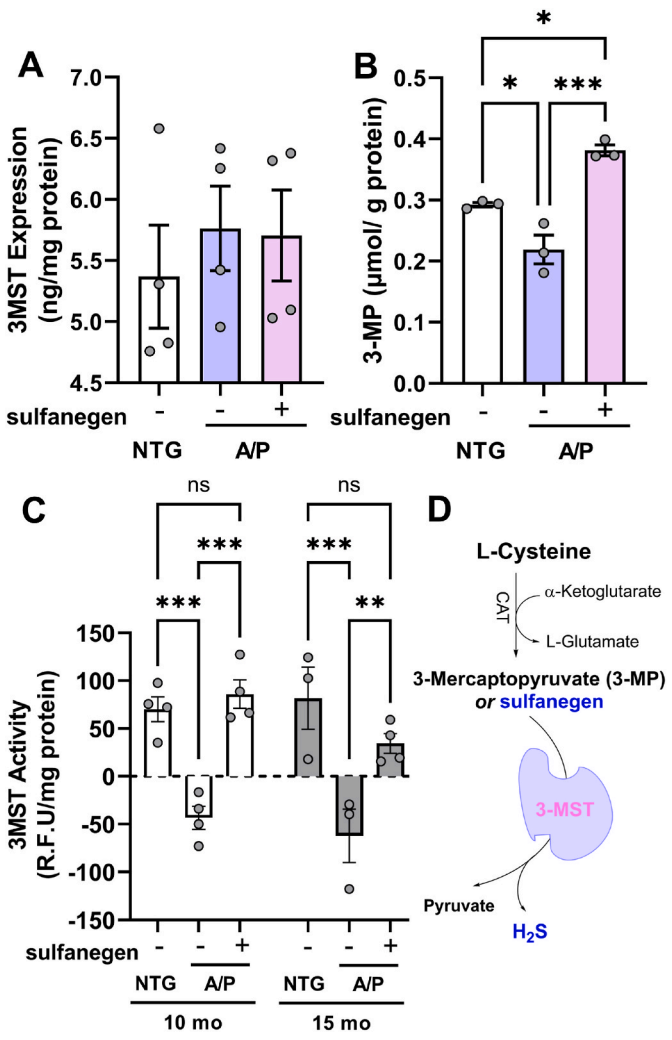

Fig. 7. Reduced 3MST function in the APP/PS1 mice is restored by sulfanegen treatment. (A) ELISA-based quantitation of 3 MST expression in the cortex region of 15 mo old cohort showed no changes in the levels of 3MST protein. (B) Quantitation of 3MST substrate, 3-mercaptopyruvate (3-MP) showed significantly reduced levels in the APP/PS1 mice, which were increased after sulfanegen treatment. (C) Endogenous activity of 3MST enzyme was significantly reduced in both 10 mo and 15 mo transgenic cohorts. Sulfanegen treatment restored 3MST function to NTG control levels. (D) 3MST enzymatic reaction showing substitution of 3-MP by sulfanegen in the enzymatic reaction, restoring its function. Statistical significance was assessed by a one-way ANOVA with Tukey's post-hoc test. $*p < 0.05$, $**p < 0.01$, $***p < 0.001$.

Declaration of competing interest

The authors declare that they have no known competing financial interests or personal relationships that could have appeared to influence the work reported in this paper. S.S.M. and R.V. are inventors on the patent application related to the use of 3-MP and its analogs as treatment options of neurodegenerative disorders.

Data availability

Data will be made available on request.

Acknowledgements

The authors would like to thank Dr. Steven Patterson for helpful discussions on sulfanegen, its synthesis and analytical method development. We greatly acknowledge technical histology help from Joyce Meints and Emmanuel Okemmatti.

Appendix A. Supplementary data

Supplementary data to this article can be found online at https://doi.org/10.1016/j.redox.2022.102484.

References

[1] A. Serrano-Pozo, M.P. Frosch, E. Masliah, B.T. Hyman, Neuropathological alterations in Alzheimer disease, Cold Spring Harb Perspect Med 1 (1) (2011) a006189, https://doi.org/10.1101/cshperspect.a006189.
[2] R. Rajmohan, P.H. Reddy, Amyloid-Beta and phosphorylated tau accumulations cause abnormalities at synapses of Alzheimer's disease neurons, J Alzheimers Dis 57 (4) (2017) 975–999, https://doi.org/10.3233/jad-160612.
[3] P. Agostinho, R.A. Cunha, C. Oliveira, Neuroinflammation, oxidative stress and the pathogenesis of Alzheimer's disease, Curr. Pharmaceut. Des. 16 (25) (2010) 2766–2778, https://doi.org/10.2174/138161210793176572.
[4] W.R. Markesbery, J.M. Carney, Oxidative alterations in Alzheimer's disease, Brain Pathol. 9 (1) (1999) 133–146, https://doi.org/10.1111/j.1750-3639.1999.tb00215.x.
[5] S. Mandrekar-Colucci, G.E. Landreth, Microglia and inflammation in Alzheimer's disease, CNS Neurol. Disord.: Drug Targets 9 (2) (2010) 156–167, https://doi.org/10.2174/187152710791012071.
[6] W.Y. Wang, M.S. Tan, J.T. Yu, L. Tan, Role of pro-inflammatory cytokines released from microglia in Alzheimer's disease, Ann. Transl. Med. 3 (10) (2015) 136, https://doi.org/10.3978/j.issn.2305-5839.2015.03.49.
[7] J.W. Kinney, S.M. Bemiller, A.S. Murtishaw, A.M. Leisgang, A.M. Salazar, B. T. Lamb, Inflammation as a central mechanism in Alzheimer's disease, Alzheimers Dement (N Y) 4 (2018) 575–590, https://doi.org/10.1016/j.trci.2018.06.014.
[8] K. Eto, T. Asada, K. Arima, T. Makifuchi, H. Kimura, Brain hydrogen sulfide is severely decreased in Alzheimer's disease, Biochem. Biophys. Res. Commun. 293 (5) (2002) 1485–1488, https://doi.org/10.1016/s0006-291x(02)00422-9.
[9] Q.H. Gong, X.R. Shi, Z.Y. Hong, L.L. Pan, X.H. Liu, Y.Z. Zhu, A new hope for neurodegeneration: possible role of hydrogen sulfide, J Alzheimers Dis 24 (Suppl 2) (2011) 173–182, https://doi.org/10.3233/jad-2011-110128.
[10] S.Q. Yang, L. Jiang, F. Lan, H.J. Wei, M. Xie, W. Zou, P. Zhang, C.Y. Wang, Y.R. Xie, X.Q. Tang, Inhibited endogenous H(2)S generation and excessive autophagy in Hippocampus contribute to sleep deprivation-induced cognitive impairment, Front. Psychol. 10 (2019) 53, https://doi.org/10.3389/fpsyg.2019.00053.
[11] E. Disbrow, K.Y. Stokes, C. Ledbetter, J. Patterson, R. Kelley, S. Pardue, T. Reekes, L. Larmeu, V. Batra, S. Yuan, U. Cvek, M. Trutschl, P. Kilgore, J.S. Alexander, C. G. Kevil, Plasma hydrogen sulfide: a biomarker of Alzheimer's disease and related dementias, Alzheimers Dement 17 (8) (2021) 1391–1402, https://doi.org/10.1002/alz.12305.
[12] X.-q. Liu, X.-q. Liu, P. Jiang, H. Huang, Y. Yan, [Plasma levels of endogenous hydrogen sulfide and homocysteine in patients with Alzheimer's disease and vascular dementia and the significance thereof], Zhonghua Yixue Zazhi 88 (32) (2008) 2246–2249.
[13] S. Chiu, A. Khan, V. Badmaev, K. Terpstra, Z. Cernovsky, J. Varghese, Z. Khazaeipool, H. Elias, A. Carriere, M. Husni, J. Copen, M. Shad, M. Woodbury-Fariña, A. Johnson, C. Chehade, Exploratory study of sublimed sulfur, in cognitively normal subjects and in Alzheimer's dementia (AD) subjects: implications for Sulfur targeting Hydrogen sulfide (H2S)/Homocysteine (Hcy) and beta-galactosidase (GALAC)/Autophagy Signaling in AD, Journal of Systems and Integrative Neuroscience 3 (2017), https://doi.org/10.15761/JSIN.1000158.
[14] H. Zhu, V. Dronamraju, W. Xie, S.S. More, Sulfur-containing therapeutics in the treatment of Alzheimer's disease, Med. Chem. Res. : an international journal for rapid communications on design and mechanisms of action of biologically active agents 30 (2) (2021) 305–352, https://doi.org/10.1007/s00044-020-02687-1.
[15] U. Shefa, M.-S. Kim, N.Y. Jeong, J. Jung, Antioxidant and cell-signaling functions of hydrogen sulfide in the central nervous system, Oxid. Med. Cell. Longev. 2018 (2018), 1873962, https://doi.org/10.1155/2018/1873962.
[16] R.Q. Li, A.R. McKinstry, J.T. Moore, B.M. Caltagarone, M.F. Eckenhoff, R. G. Eckenhoff, M.B. Kelz, Is hydrogen sulfide-induced suspended animation general anesthesia? J. Pharmacol. Exp. Therapeut. 341 (3) (2012) 735–742, https://doi.org/10.1124/jpet.111.187237.
[17] M.R. Filipovic, J. Zivanovic, B. Alvarez, R. Banerjee, Chemical biology of H2S signaling through persulfidation, Chem. Rev. 118 (3) (2018) 1253–1337, https://doi.org/10.1021/acs.chemrev.7b00205.
[18] Y. Kimura, Y. Goto, H. Kimura, Hydrogen sulfide increases glutathione production and suppresses oxidative stress in mitochondria, Antioxidants Redox Signal. 12 (1) (2010) 1–13, https://doi.org/10.1089/ars.2008.2282.
[19] G. Qi-Hai, W. Qian, P. Li-Long, L. Xin-Hua, H. Hui, Z. Yi-Zhun, Hydrogen sulfide attenuates lipopolysaccharide-induced cognitive impairment: a pro-inflammatory pathway in rats, Pharmacol. Biochem. Behav. 96 (1) (2010) 52–58, https://doi.org/10.1016/j.pbb.2010.04.006.
[20] L.F. Hu, P.T.H. Wong, P.K. Moore, J.S. Bian, Hydrogen sulfide attenuates lipopolysaccharide-induced inflammation by inhibition of p38 mitogen-activated protein kinase in microglia, J. Neurochem. 100 (4) (2007) 1121–1128, https://doi.org/10.1111/j.1471-4159.2006.04283.x.
[21] X.Q. Tang, C.T. Yang, J. Chen, W.L. Yin, S.W. Tian, B. Hu, J.Q. Feng, Y.J. Li, Effect of hydrogen sulphide on β-amyloid-induced damage in PC12 cells, Clin. Exp.

Pharmacol. Physiol. 35 (2) (2008) 180–186, https://doi.org/10.1111/j.1440-1681.2007.04799.x.
[22] D. Petrovic, E. Kouroussis, T. Vignane, M.R. Filipovic, The role of protein persulfidation in brain aging and neurodegeneration, Front. Aging Neurosci. 13 (2021), 674135, https://doi.org/10.3389/fnagi.2021.674135.
[23] B.D. Paul, Neuroprotective roles of the reverse transsulfuration pathway in Alzheimer's disease, Front. Aging Neurosci. 13 (2021), 659402, https://doi.org/10.3389/fnagi.2021.659402.
[24] Y. Liu, Y. Deng, H. Liu, C. Yin, X. Li, Q. Gong, Hydrogen sulfide ameliorates learning memory impairment in APP/PS1 transgenic mice: a novel mechanism mediated by the activation of Nrf2, Pharmacol. Biochem. Behav. 150–151 (2016) 207–216, https://doi.org/10.1016/j.pbb.2016.11.002.
[25] D. Giovinazzo, B. Bursac, I. Sbodio Juan, S. Nalluru, T. Vignane, M. Snowman Adele, M. Albacarys Lauren, W. Sedlak Thomas, R. Torregrossa, M. Whiteman, R. Filipovic Milos, H. Snyder Solomon, D. Paul Bindu, Hydrogen sulfide is neuroprotective in Alzheimer's disease by sulfhydrating GSK3β and inhibiting Tau hyperphosphorylation, Proc. Natl. Acad. Sci. USA 118 (4) (2021), e2017225118, https://doi.org/10.1073/pnas.2017225118.
[26] A. Xuan, D. Long, J. Li, W. Ji, M. Zhang, L. Hong, J. Liu, Hydrogen sulfide attenuates spatial memory impairment and hippocampal neuroinflammation in beta-amyloid rat model of Alzheimer's disease, J. Neuroinflammation 9 (1) (2012) 202, https://doi.org/10.1186/1742-2094-9-202.
[27] A. Lan, W. Xu, H. Zhang, X. Hua, D. Zheng, R. Guo, N. Shen, F. Hu, J. Feng, D. Liu, Inhibition of ROS-activated p38MAPK pathway is involved in the protective effect of H2S against chemical hypoxia-induced inflammation in PC12 cells, Neurochem. Res. 38 (7) (2013) 1454–1466, https://doi.org/10.1007/s11064-013-1044-x.
[28] J.I. Sbodio, S.H. Snyder, B.D. Paul, Golgi stress response reprograms cysteine metabolism to confer cytoprotection in Huntington's disease, Proc. Natl. Acad. Sci. U. S. A. 115 (4) (2018) 780–785, https://doi.org/10.1073/pnas.1717877115.
[29] C. Hine, E. Harputlugil, Y. Zhang, C. Ruckenstuhl, B.C. Lee, L. Brace, A. Longchamp, J.H. Treviño-Villarreal, P. Mejia, C.K. Ozaki, R. Wang, V. N. Gladyshev, F. Madeo, W.B. Mair, J.R. Mitchell, Endogenous hydrogen sulfide production is essential for dietary restriction benefits, Cell 160 (1–2) (2015) 132–144, https://doi.org/10.1016/j.cell.2014.11.048.
[30] N. Shibuya, M. Tanaka, M. Yoshida, Y. Ogasawara, T. Togawa, K. Ishii, H. Kimura, 3-Mercaptopyruvate sulfurtransferase produces hydrogen sulfide and bound sulfane sulfur in the brain, Antioxidants Redox Signal. 11 (4) (2009) 703–714, https://doi.org/10.1089/ars.2008.2253.
[31] X. Chen, K.-H. Jhee, W.D. Kruger, Production of the neuromodulator H2S by cystathionine β-synthase via the condensation of cysteine and homocysteine, J. Biol. Chem. 279 (50) (2004) 52082–52086, https://doi.org/10.1074/jbc.C400481200.
[32] T. Morikawa, M. Kajimura, T. Nakamura, T. Hishiki, T. Nakanishi, Y. Yukutake, Y. Nagahata, M. Ishikawa, K. Hattori, T. Takenouchi, T. Takahashi, I. Ishii, K. Matsubara, Y. Kabe, S. Uchiyama, E. Nagata, M.M. Gadalla, S.H. Snyder, M. Suematsu, Hypoxic regulation of the cerebral microcirculation is mediated by a carbon monoxide-sensitive hydrogen sulfide pathway, Proc. Natl. Acad. Sci. U. S. A. 109 (4) (2012) 1293–1298, https://doi.org/10.1073/pnas.1119658109.
[33] O. Kabil, R. Banerjee, Enzymology of H2S biogenesis, decay and signaling, Antioxidants Redox Signal. 20 (5) (2014) 770–782, https://doi.org/10.1089/ars.2013.5339.
[34] Y. Enokido, E. Suzuki, K. Iwasawa, K. Namekata, H. Okazawa, H. Kimura, Cystathionine beta-synthase, a key enzyme for homocysteine metabolism, is preferentially expressed in the radial glia/astrocyte lineage of developing mouse CNS, Faseb. J. 19 (13) (2005) 1854–1856, https://doi.org/10.1096/fj.05-3724fje.
[35] K. Robert, F. Vialard, E. Thiery, K. Toyama, P.M. Sinet, N. Janel, J. London, Expression of the cystathionine beta synthase (CBS) gene during mouse development and immunolocalization in adult brain, J. Histochem. Cytochem. 51 (3) (2003) 363–371, https://doi.org/10.1177/002215540305100311.
[36] N. Denoix, T. Merz, S. Unmuth, A. Hoffmann, E. Nespoli, A. Scheuerle, M. Huber-Lang, H. Gündel, C. Waller, P. Radermacher, O. McCook, Cerebral immunohistochemical characterization of the H2S and the oxytocin systems in a porcine model of acute subdural hematoma, Front. Neurol. 11 (2020), https://doi.org/10.3389/fneur.2020.00649.
[37] H. Zhao, S.-J. Chan, Y.-K. Ng, P.T.H. Wong, Brain 3-mercaptopyruvate sulfurtransferase (3MST): cellular localization and downregulation after acute stroke, PLoS One 8 (6) (2013), e67322, https://doi.org/10.1371/journal.pone.0067322.
[38] B.-B. Tao, S.-Y. Liu, C.-C. Zhang, W. Fu, W.-J. Cai, Y. Wang, Q. Shen, M.-J. Wang, Y. Chen, L.-J. Zhang, Y.-Z. Zhu, Y.-C. Zhu, VEGFR2 functions as an H2S-targeting receptor protein kinase with its novel cys1045–cys1024 disulfide bond serving as a specific molecular switch for hydrogen sulfide actions in vascular endothelial cells, Antioxidants Redox Signal. 19 (5) (2012) 448–464, https://doi.org/10.1089/ars.2012.4565.
[39] K.R. Olson, K.D. Straub, The role of hydrogen sulfide in evolution and the evolution of hydrogen sulfide in metabolism and signaling, Physiology 31 (1) (2016) 60–72, https://doi.org/10.1152/physiol.00024.2015.
[40] B. Fräsdorf, C. Radon, S. Leimkühler, Characterization and interaction studies of two isoforms of the dual localized 3-mercaptopyruvate sulfurtransferase TUM1 from humans, J. Biol. Chem. 289 (50) (2014) 34543–34556, https://doi.org/10.1074/jbc.M114.605733.
[41] A. Koj, J. Frendo, L. Wojtczak, Subcellular distribution and intramitochondrial localization of three sulfurtransferases in rat liver, FEBS (Fed. Eur. Biochem. Soc.) Lett. 57 (1) (1975) 42–46, https://doi.org/10.1016/0014-5793(75)80148-7.
[42] M. Tomita, N. Nagahara, T. Ito, Expression of 3-mercaptopyruvate sulfurtransferase in the mouse, Molecules 21 (12) (2016), https://doi.org/10.3390/molecules21121707.
[43] F. Zhang, S. Chen, J.-Y. Wen, Z.-W. Chen, 3-Mercaptopyruvate sulfurtransferase/hydrogen sulfide protects cerebral endothelial cells against oxygen-glucose deprivation/reoxygenation-induced injury via mitoprotection and inhibition of the RhoA/ROCK pathway, Am. J. Physiol. Cell Physiol. 319 (4) (2020) C720–C733, https://doi.org/10.1152/ajpcell.00014.2020.
[44] S.E. Patterson, B. Moeller, H.T. Nagasawa, R. Vince, D.L. Crankshaw, J. Briggs, M. W. Stutelberg, C.V. Vinnakota, B.A. Logue, Development of sulfanegen for mass cyanide casualties, Ann. N. Y. Acad. Sci. 1374 (1) (2016) 202–209, https://doi.org/10.1111/nyas.13114.
[45] S.E. Patterson, A.R. Monteil, J.F. Cohen, D.L. Crankshaw, R. Vince, H.T. Nagasawa, Cyanide antidotes for mass casualties: water-soluble salts of the dithiane (sulfanegen) from 3-mercaptopyruvate for intramuscular administration, J. Med. Chem. 56 (3) (2013) 1346–1349, https://doi.org/10.1021/jm301633x.
[46] K.G. Belani, H. Singh, D.S. Beebe, P. George, S.E. Patterson, H.T. Nagasawa, R. Vince, Cyanide toxicity in juvenile pigs and its reversal by a new prodrug, sulfanegen sodium, Anesth. Analg. 114 (5) (2012) 956–961, https://doi.org/10.1213/ANE.0b013e31824c4eb5.
[47] M. Brenner, J.G. Kim, J. Lee, S.B. Mahon, D. Lemor, R. Ahdout, G.R. Boss, W. Blackledge, L. Jann, H.T. Nagasawa, S.E. Patterson, Sulfanegen sodium treatment in a rabbit model of sub-lethal cyanide toxicity, Toxicol. Appl. Pharmacol. 248 (3) (2010) 269–276, https://doi.org/10.1016/j.taap.2010.08.002.
[48] M.W. Stutelberg, A.R. Monteil, K.G. Belani, B. Moeller, H. Singh, N. Kaur, S.S. Sra, D.S. Beebe, S.E. Patterson, B.A. Logue, Pharmacokinetics of next generation cyanide antidote sulfanegen in rabbits, International Journal of Pharmacokinetics 2 (2) (2017) 105–111, https://doi.org/10.4155/ipk-2016-0021.
[49] S.S. More, R. Vince, Potential of a γ-glutamyl-transpeptidase-stable glutathione analogue against amyloid-β toxicity, ACS Chem. Neurosci. 3 (3) (2012) 204–210, https://doi.org/10.1021/cn200113z.
[50] S.B. Kedare, R.P. Singh, Genesis and development of DPPH method of antioxidant assay, J. Food Sci. Technol. 48 (4) (2011) 412–422, https://doi.org/10.1007/s13197-011-0251-1.
[51] R.V. Kartha, J. Zhou, L.B. Hovde, B.W. Cheung, H. Schröder, Enhanced detection of hydrogen sulfide generated in cell culture using an agar trap method, Anal. Biochem. 423 (1) (2012) 102–108, https://doi.org/10.1016/j.ab.2012.01.001.
[52] C. Coletta, K. Módis, B. Szczesny, A. Brunyánszki, G. Oláh, E.C.S. Rios, K. Yanagi, A. Ahmad, A. Papapetropoulos, C. Szabo, Regulation of vascular tone, angiogenesis and cellular bioenergetics by the 3-mercaptopyruvate sulfurtransferase/H2S pathway: functional impairment by hyperglycemia and restoration by DL-α-lipoic acid, Mol. Med. 21 (1) (2015) 1–14, https://doi.org/10.2119/molmed.2015.00035.
[53] V.S. Lin, A.R. Lippert, C.J. Chang, Cell-trappable fluorescent probes for endogenous hydrogen sulfide signaling and imaging H2O2-dependent H2S production, Proc. Natl. Acad. Sci. U.S.A. 110 (18) (2013) 7131–7135, https://doi.org/10.1073/pnas.1302193110.
[54] W. Xie, K.H. Kim, R. Vince, S.S. More, The amyloid aggregation accelerator diacetyl prevents cognitive decline in Alzheimer's mouse models, Chem. Res. Toxicol. 34 (5) (2021) 1355–1366, https://doi.org/10.1021/acs.chemrestox.1c00089.
[55] Y.I. Christopher Kwon, W. Xie, H. Zhu, J. Xie, K. Shinn, N. Juckel, R. Vince, S. S. More, M.K. Lee, γ-Glutamyl-Transpeptidase-Resistant glutathione analog attenuates progression of Alzheimer's disease-like pathology and neurodegeneration in a mouse model, Antioxidants 10 (11) (2021) 1796, https://doi.org/10.3390/antiox10111796.
[56] P.R. Mouton, A.M. Gokhale, N.L. Ward, M.J. West, Stereological length estimation using spherical probes, J. Microsc. 206 (Pt 1) (2002) 54–64, https://doi.org/10.1046/j.1365-2818.2002.01006.x.
[57] G. Paxinos, K.B. Franklin, The Mouse Brain in Stereotaxic Coordinates, Third., Academic Press, 2008.
[58] Y. Liu, M.-J. Yoo, A. Savonenko, W. Stirling, D.L. Price, D.R. Borchelt, L. Mamounas, W.E. Lyons, M.E. Blue, M.K. Lee, Amyloid pathology is associated with progressive monoaminergic neurodegeneration in a transgenic mouse model of Alzheimer's disease, J. Neurosci. 28 (51) (2008) 13805–13814, https://doi.org/10.1523/JNEUROSCI.4218-08.2008.
[59] K. Hanaoka, K. Sasakura, Y. Suwanai, S. Toma-Fukai, K. Shimamoto, Y. Takano, N. Shibuya, T. Terai, T. Komatsu, T. Ueno, Y. Ogasawara, Y. Tsuchiya, Y. Watanabe, H. Kimura, C. Wang, M. Uchiyama, H. Kojima, T. Okabe, Y. Urano, T. Shimizu, T. Nagano, Discovery and mechanistic characterization of selective inhibitors of H(2)S-producing enzyme: 3-mercaptopyruvate sulfurtransferase (3MST) targeting active-site cysteine persulfide, Sci. Rep. 7 (2017), https://doi.org/10.1038/srep40227, 40227-40227.
[60] Q.H. Gong, L.L. Pan, X.H. Liu, Q. Wang, H. Huang, Y.Z. Zhu, S-propargyl-cysteine (ZYZ-802), a sulphur-containing amino acid, attenuates beta-amyloid-induced cognitive deficits and pro-inflammatory response: involvement of ERK1/2 and NF-κB pathway in rats, Amino Acids 40 (2) (2011) 601–610, https://doi.org/10.1007/s00726-010-0685-1.
[61] I. Loryan, A. Reichel, B. Feng, C. Bundgaard, C. Shaffer, C. Kalvass, D. Bednarczyk, D. Morrison, D. Lesuisse, E. Hoppe, G.C. Terstappen, H. Fischer, L. Di, N. Colclough, S. Summerfield, S.T. Buckley, T.S. Maurer, M. Fridén, Unbound brain-to-plasma partition coefficient, kp,uu,brain—a game changing parameter for CNS drug discovery and development, Pharmaceut. Res. (2022), https://doi.org/10.1007/s11095-022-03246-6.

[62] M.A. DeTure, D.W. Dickson, The neuropathological diagnosis of Alzheimer's disease, Mol. Neurodegener. 14 (1) (2019) 32, https://doi.org/10.1186/s13024-019-0333-5.
[63] D.P. Perl, Neuropathology of Alzheimer's disease, Mt. Sinai J. Med. 77 (1) (2010) 32–42, https://doi.org/10.1002/msj.20157.
[64] A. Serrano-Pozo, M.P. Frosch, E. Masliah, B.T. Hyman, Neuropathological alterations in Alzheimer disease, Cold Spring Harbor perspectives in medicine 1 (1) (2011), https://doi.org/10.1101/cshperspect.a006189 a006189-a006189.
[65] E. Vandini, A. Ottani, D. Zaffe, A. Calevro, F. Canalini, G.M. Cavallini, R. Rossi, S. Guarini, D. Giuliani, Mechanisms of hydrogen sulfide against the progression of severe Alzheimer's disease in transgenic mice at different ages, Pharmacology 103 (1–2) (2019) 50–60, https://doi.org/10.1159/000494113.
[66] M. Izco, P. Martinez, A. Corrales, N. Fandos, S. Garcia, D. Insua, M. Montanes, V. Perez-Grijalba, N. Rueda, V. Vidal, Changes in the brain and plasma Aβ peptide levels with age and its relationship with cognitive impairment in the APPswe/PS1dE9 mouse model of Alzheimer's disease, Neuroscience 263 (2014) 269–279.
[67] S.S. More, A.P. Vartak, R. Vince, Restoration of glyoxalase enzyme activity precludes cognitive dysfunction in a mouse model of Alzheimer's disease, ACS Chem. Neurosci. 4 (2) (2013) 330–338, https://doi.org/10.1021/cn3001679.
[68] Y. Kimura, H. Kimura, Hydrogen sulfide protects neurons from oxidative stress, FASEB (Fed. Am. Soc. Exp. Biol.) J. 18 (10) (2004) 1165–1167, https://doi.org/10.1096/fj.04-1815fje.
[69] Q.H. Gong, Q. Wang, L.L. Pan, X.H. Liu, H. Xin, Y.Z. Zhu, S-Propargyl-cysteine, a novel hydrogen sulfide-modulated agent, attenuates lipopolysaccharide-induced spatial learning and memory impairment: involvement of TNF signaling and NF-κB pathway in rats, Brain Behav. Immun. 25 (1) (2011) 110–119, https://doi.org/10.1016/j.bbi.2010.09.001.
[70] A.J. Ehrenberg, A.K. Nguy, P. Theofilas, S. Dunlop, C.K. Suemoto, A.T. Di Lorenzo Alho, R.P. Leite, R. Diehl Rodriguez, M.B. Mejia, U. Rüb, J.M. Farfel, R.E. de Lucena Ferretti-Rebustini, C.F. Nascimento, R. Nitrini, C.A. Pasqualucci, W. Jacob-Filho, B. Miller, W.W. Seeley, H. Heinsen, L.T. Grinberg, Quantifying the accretion of hyperphosphorylated tau in the locus coeruleus and dorsal raphe nucleus: the pathological building blocks of early Alzheimer's disease, Neuropathol. Appl. Neurobiol. 43 (5) (2017) 393–408, https://doi.org/10.1111/nan.12387.
[71] P. Theofilas, A.J. Ehrenberg, S. Dunlop, A.T. Di Lorenzo Alho, A. Nguy, R.E. P. Leite, R.D. Rodriguez, M.B. Mejia, C.K. Suemoto, R.E.D.L. Ferretti-Rebustini, L. Polichiso, C.F. Nascimento, W.W. Seeley, R. Nitrini, C.A. Pasqualucci, W. Jacob Filho, U. Rueb, J. Neuhaus, H. Heinsen, L.T. Grinberg, Locus coeruleus volume and cell population changes during Alzheimer's disease progression: a stereological study in human postmortem brains with potential implication for early-stage biomarker discovery, Alzheimers Dement 13 (3) (2017) 236–246, https://doi.org/10.1016/j.jalz.2016.06.2362.
[72] S. Sestito, S. Daniele, D. Pietrobono, V. Citi, L. Bellusci, G. Chiellini, V. Calderone, C. Martini, S. Rapposelli, Memantine prodrug as a new agent for Alzheimer's Disease, Sci. Rep. 9 (1) (2019) 4612, https://doi.org/10.1038/s41598-019-40925-8.
[73] T. Panagaki, E.B. Randi, C. Szabo, Role of 3-mercaptopyruvate sulfurtransferase in the regulation of proliferation and cellular bioenergetics in human down syndrome fibroblasts, Biomolecules 10 (4) (2020) 653, https://doi.org/10.3390/biom10040653.